AGU PUBLICATIONS

Global Biogeochemical Cycles

RESEARCH ARTICLE
10.1002/2014GB004833

**Key Points:**
- Late summer NCP in the central Arctic Ocean by multiple approaches
- High NCP in the marginal sea ice zone and low NCP in the central basins
- Basin-specific variability coupled to sea ice cover and nutrient supply

**Supporting Information:**
- Readme
- Figure S1
- Figure S2
- Figure S3
- Figure S4
- Table S1
- Table S2
- Table S3
- Table S4
- Table S5
- Table S6

**Correspondence to:**
A. Ulfsbo,
ulfsbo@chem.gu.se

**Citation:**
Ulfsbo, A., N. Cassar, M. Korhonen, S. van Heuven, M. Hoppema, G. Kattner, and L. G. Anderson (2014), Late summer net community production in the central Arctic Ocean using multiple approaches, *Global Biogeochem. Cycles*, *28*, 1129–1148 doi:10.1002/2014GB004833.

Received 17 FEB 2014
Accepted 19 SEP 2014
Accepted article online 24 SEP 2014
Published online 25 OCT 2014

# Late summer net community production in the central Arctic Ocean using multiple approaches

**Adam Ulfsbo[1], Nicolas Cassar[2], Meri Korhonen[3,4], Steven van Heuven[5], Mario Hoppema[6], Gerhard Kattner[6], and Leif G. Anderson[1]**

[1]Department of Chemistry and Molecular Biology, University of Gothenburg, Gothenburg, Sweden, [2]Division of Earth and Ocean Sciences, Nicholas School of the Environment, Duke University, Durham, North Carolina, USA, [3]Finnish Meteorological Institute, Helsinki, Finland, [4]Department of Physics, University of Helsinki, Helsinki, Finland, [5]Centre for Isotope Research, University of Groningen, Groningen, Netherlands, [6]Alfred Wegener Institute Helmholtz Centre for Polar and Marine Research, Bremerhaven, Germany

**Abstract** Large-scale patterns of net community production (NCP) were estimated during the late summer cruise ARK-XXVI/3 (TransArc, August/September 2011) to the central Arctic Ocean. Several approaches were used based on the following: (i) continuous measurements of surface water oxygen to argon ratios ($O_2$/Ar), (ii) underway measurements of surface partial pressure of carbon dioxide ($pCO_2$), (iii) discrete samples of dissolved inorganic carbon, and (iv) dissolved inorganic nitrogen and phosphate. The NCP estimates agreed well within the uncertainties associated with each approach. The highest late summer NCP (up to 6 mol C $m^{-2}$) was observed in the marginal sea ice zone region. Low values (<1 mol C $m^{-2}$) were found in the sea ice-covered deep basins with a strong spatial variability. Lowest values were found in the Amundsen Basin and moderate values in the Nansen and Makarov Basins with slightly higher estimates over the Mendeleev Ridge. Our findings support a coupling of NCP to sea ice coverage and nutrient supply and thus stress a potential change in spatial and temporal distribution of NCP in a future Arctic Ocean. To follow the evolution of NCP in space and time, it is suggested to apply one or several of these approaches in shipboard investigations with a time interval of 3 to 5 years.

## 1. Introduction

The central Arctic Ocean and its adjacent shelf seas are a system in transition under the influence of natural and anthropogenic processes. These include the declining summer sea ice extent, with the record minimum in September 2012 [*Laxon et al*., 2013], and the warming of its surface waters [*Steele et al*., 2008]. Other physical changes have been reported [*Karcher et al*., 2012; *McGuire et al*., 2006; *Morison et al*., 2012; *Nicolaus et al*., 2012], as well as shifts in Arctic ecosystems [*Arrigo et al*., 2008; *Li et al*., 2009; *Pabi et al*., 2008]. Combined, these changes are likely to affect the Arctic primary production regime [*Tremblay and Gagnon*, 2009] although it is not possible to say to what extent and in which direction.

The Arctic Ocean takes up substantial amounts of carbon dioxide ($CO_2$) from the atmosphere annually, thus having an important influence on the global carbon cycle [*Bates and Mathis*, 2009; *Macdonald et al*., 2009]. The anthropogenic carbon inventory of the intermediate layers has increased during the last two decades [*Ericson et al*., 2014], and the anthropogenic $CO_2$ concentration of the Arctic Ocean is nearly twice that of the global mean [*Tanhua et al*., 2009]. Vertical transport of carbon to the deep central Arctic Ocean is promoted by convective ventilation of subsurface waters. This results from the cooling of warm inflowing surface waters [e.g., *Mauritzen*, 1996] and brine release during sea ice formation [*Anderson et al*., 2004a; *Else et al*., 2011]. In contrast, there is a notion of very low export fluxes of organic matter to the deep basins [*Anderson et al*., 2003; *Cai et al*., 2010].

It is unclear whether the Arctic Ocean, under summer ice-free conditions, will remain a large sink for atmospheric $CO_2$ [*Bates and Mathis*, 2009], will become a moderate sink [*Cai et al*., 2010], or that it even will become a $CO_2$ source [*Steiner et al*., 2013]. The outcome will depend on the future changes in primary and carbon export production and may be different for different regions. Our capability to predict the changing character of the Arctic Ocean thus requires a thorough understanding of the current state and processes governing primary and export production.

Export of organic carbon from the surface layer depends on, among other things, the net community production (NCP). NCP is the difference between gross primary production and the community's combined autotrophic

and heterotrophic respiration. Since storage of organic carbon in the mixed layer is likely to be modest with respect to NCP over large spatial and temporal scales, NCP approximates carbon export production [*Falkowski et al*., 2003]. Most studies of primary production and NCP in the Arctic Ocean have focused on the productive marginal seas, particularly the Barents and Bering Seas [e.g., *Cross et al*., 2012; *Sakshaug*, 2004; *Shadwick et al*., 2011; *Wassmann et al*., 2006]. This is in part due to the inaccessibility of the central Arctic Ocean. Current estimates of annual or seasonal average primary production and NCP for the ice-covered deep basins of the central Arctic Ocean are generally low compared to the adjacent shelf seas [*Anderson et al*., 2003; *Codispoti et al*., 2013; *Sakshaug*, 2004]. Recent studies based on satellite monitoring have suggested an increase in net primary production (i.e., gross primary production minus autotrophic respiration) during the period 1998 to 2009, likely as a result of the shrinking sea ice cover [*Arrigo and van Dijken*, 2011]. Massive phytoplankton blooms have lately been observed under the Arctic sea ice [*Arrigo et al*., 2012] as well as unprecedented, widespread export and deposition of algal biomass from the melting sea ice [*Boetius et al*., 2013].

Primary production in the central Arctic Ocean is primarily limited by light and nutrients [*Popova et al*., 2010; *Sakshaug*, 2004; *Vancoppenolle et al*., 2013]. The high-latitude seasonal light regime constrains the timing and duration of the growing season. Light transmittance into the surface ocean is strongly influenced by ice concentration, ice thickness and type, and snow cover [*Nicolaus et al*., 2012]. With a declining sea ice extent, annual Arctic primary production is expected to increase due to a greater area exposed to light, leading to a longer growing season [*Arrigo et al*., 2008] if nutrients are available. In a more open Arctic Ocean, nutrients may become the more important limiting factor [*Tremblay and Gagnon*, 2009], although wind-driven upwelling of nutrient-rich deep waters is expected to increase shelf production [*Carmack and Chapman*, 2003]. The input of nutrients into the photic zone is governed by the strong density stratification of the mixed layer, ocean mixing, upwelling, eddy events and by the nutrient concentrations of the different source waters [e.g., *Codispoti et al*., 2013].

The seasonal NCP can be estimated from the drawdown (depletions or deficits) of inorganic matter in the surface ocean. This approach has been applied in the central Arctic Ocean and its marginal seas, using either seasonal data [*Mathis et al*., 2010; *Shadwick et al*., 2011] or estimates of fractions and preformed concentrations of the different source waters entering the Arctic Ocean [*Anderson et al*., 2003; *Fransson et al*., 2001].

To better constrain the NCP in the central Arctic Ocean, we expand these approaches to assess the large-scale distribution, magnitude, and variability of the NCP, using data acquired during late summer 2011. We exploit several approaches based on (i) continuous measurements of surface water oxygen to argon ratios ($O_2$/Ar), (ii) surface water $pCO_2$, (iii) discrete samples of dissolved inorganic carbon (DIC), and (iv) dissolved inorganic nitrogen and phosphate. Our measurements provide a quantitative documentation of the current state to assess potential future changes in an Arctic Ocean with decreasing summer sea ice extent.

## 2. Oceanographic Setting

The oceanographic setting is critical to primary production in the Arctic Ocean and to the computation of NCP by the different methods presented below. The water circulation below the halocline is largely topographically driven, with cyclonic circulation within the four deep basins: the Nansen, Amundsen, Canada, and Makarov Basins [*Rudels et al*., 1994] (Figure 1). The waters feeding into the subsurface layers of these basins come from the Atlantic Ocean and enter both through Fram Strait and via the Barents Sea. The surface water circulation pattern is divided into two major regimes: one large anticyclonic circulation in the Canada and Makarov Basins, i.e., the Beaufort Gyre, and one more direct flow of water from the Siberian Shelf region toward Fram Strait via the Nansen and Amundsen Basins [*Jones et al*., 1998]. The boundary between these two circulation patterns varies with time and is determined by the large-scale atmospheric pressure field [*Bourgain et al*., 2013].

The horizontal supply of water to the surface layers of the central basins is both from the Pacific Ocean through the Bering Sea and from the Atlantic Ocean along the continental shelf seas all the way to the East Siberian Sea. Added to this are vast amounts of river water, which have a strong seasonal signal with low input in winter and a strong spring flood. For example, the average nitrate concentration of six large rivers (Ob, Yenisey, Lena, Kolyma, Yukon, and Mackenzie) is ~3 μM in the summer and ~14 μM in the winter [*Holmes et al*., 2012] with an annual mean of ~6 μM. Total dissolved phosphate is ~0.6 μM and does not vary much throughout the year. The long residence time of several years of the water on the shelves [*Ekwurzel et al*., 2001; *Popova et al*., 2013] attenuates this seasonal signal within the deep central basins.

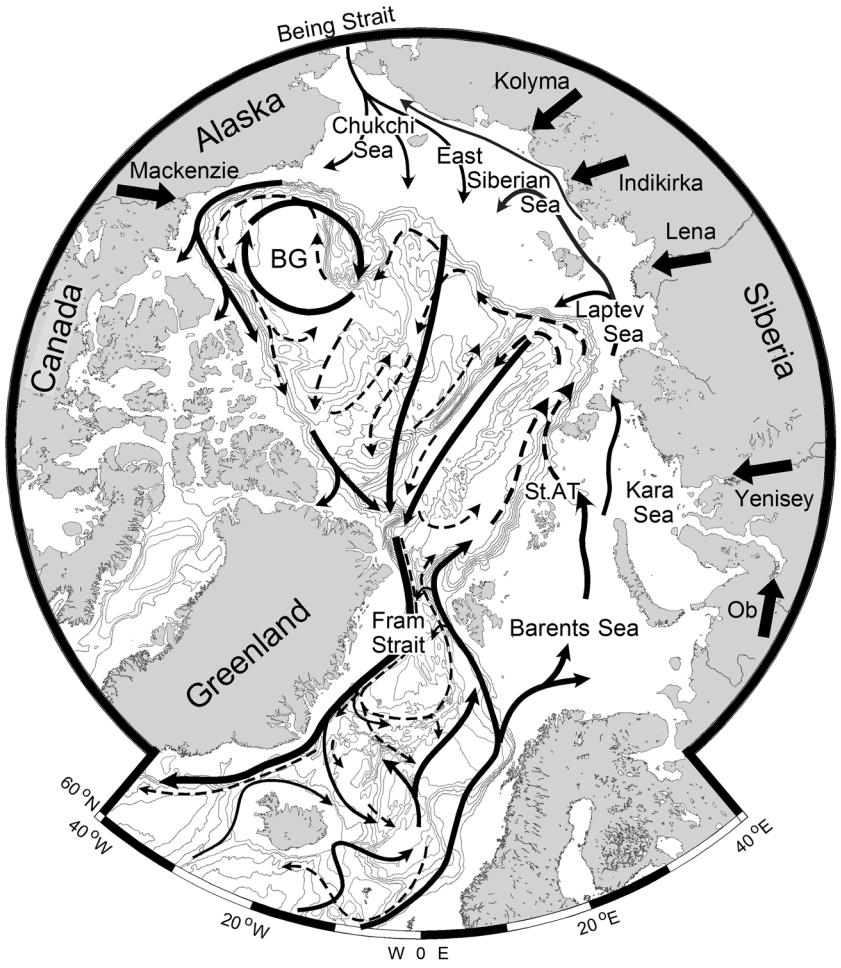


**Figure 1.** General Arctic Ocean circulation together with the dominating rivers entering this domain. Surface currents are illustrated by solid lines, while the deep currents are represented by dashed lines (modified after *Rudels et al.* [1994]).

Farther offshore, away from the shelf seas, a seasonal signal in the salinity of the surface water originates from melting sea ice in summer and freezing during winter. Brine release by sea ice formation triggers convection which leads to a homogeneous winter mixed layer. This layer has a depth that varies from more than 100 m north of the Barents Sea where the Atlantic water enters the deep Arctic Ocean, to less than 50 m in the central regions [*Rudels et al.*, 1996]. The exact depth of the surface winter mixed layer varies annually depending on the production of sea ice. During summer, sea ice melt contributes in forming a summer halocline. The waters above the summer halocline are homogenized by mechanical mixing induced by wind stress and ice drag, giving rise to a summer mixed layer. The mechanical mixing does not reach as deep as the convection triggered by density increase, and thus, the summer mixed layer is much shallower than the winter mixed layer.

During winter, the homogenization of the upper water column contributes to nutrient availability at the beginning of the next productive season. Nutrients are additionally supplied by inflow from the Atlantic and Pacific Oceans, where the latter exhibits higher concentrations. Riverine nutrient input differs amongst the large Arctic rivers [e.g., *Holmes et al.*, 2012], is partially consumed within the vast shelf seas and will thus not add to the surface waters of the central basins. The halocline of the central basins is supplied by shelf bottom waters, which have a strong signal of organic matter remineralization. This water, known as the upper halocline, is mainly confined to the Pacific sector of the Arctic Ocean, with its presence in the Atlantic sector depending on the atmospheric pressure field. Depending on the wind and sea ice conditions over the continental margins, the upper halocline water can be mixed up into the surface during extreme events [*Carmack and Chapman*, 2003], thus adding nutrients to the photic zone.

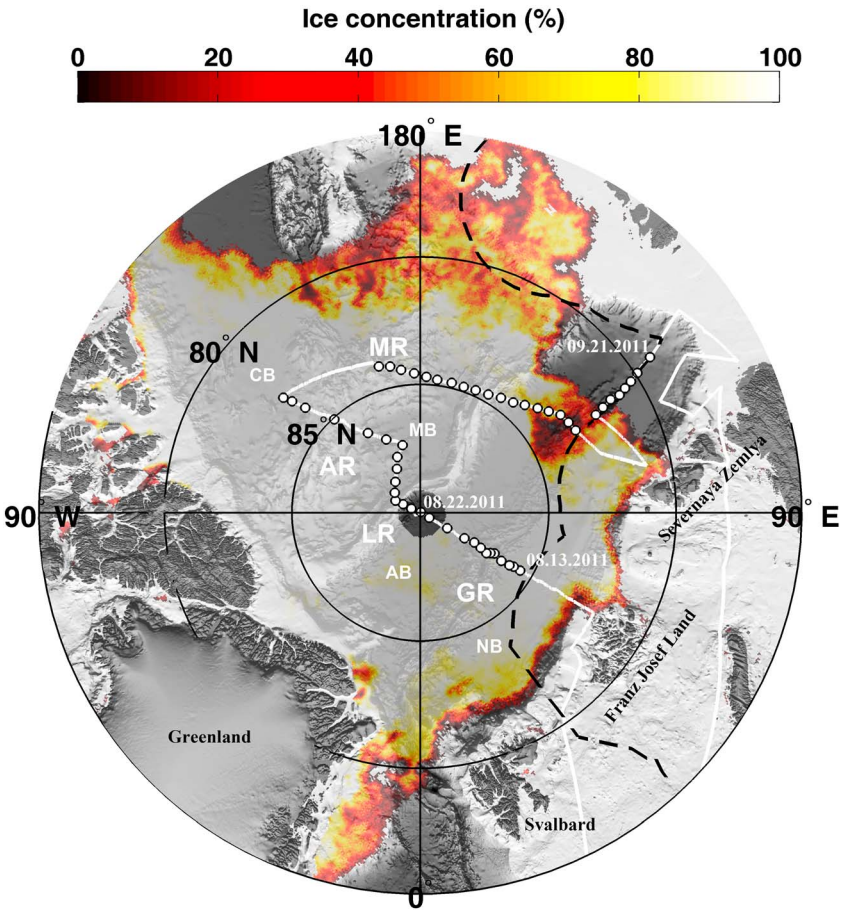


**Figure 2.** Cruise track (white line) and CTD stations (white circles) occupied during ARK-XXVI/3 in the central Arctic Ocean 2011. The first biogeochemical CTD station in the Nansen Basin was occupied on 13 August, reaching 90°N on 22 August, and the last station toward the Laptev Sea on 21 September. The dashed black line indicates the Russian Exclusive Economic Zone [*VLIZ*, 2011]. The ice concentration (transparent) is a snapshot from 7 September 2011 (as derived from Advanced Microwave Scanning Radiometer–EOS (AMSR-E) (89 GHz), 6.25 km, University of Bremen). The bathymetry is from ETOPO1 1 arc min data [*Amante and Eakins*, 2009]. Abbreviations are Nansen Basin (NB), Amundsen Basin (AB), Canada Basin (CB), Makarov Basin (MB), Gakkel Ridge (GR), Lomonosov Ridge (LR), Alpha Ridge (AR), and Mendeleev Ridge (MR).

## 3. Methods

### 3.1. Sampling

Discrete samples were collected and analyzed onboard the R/V *Polarstern* during the transpolar cruise ARK-XXVI/3 (TransArc) from 5 August (Tromsø, Norway) to 7 October (Bremerhaven, Germany) in 2011 [*Schauer*, 2012]. A standard conductivity-temperature-depth (CTD)/rosette water sampler system (Seabird® SBE9+ CTD/SBE32, 24 × 12 L Niskin bottles) was deployed at 111 stations. Of these, 53 stations yielded a complete data set of physical and biogeochemical properties including pressure, salinity, temperature, oxygen, fluorescence [*Schauer et al*., 2011]; DIC, total alkalinity (TA), and pH [*Anderson et al*., 2011]; as well as nitrate, nitrite, ammonium, phosphate, and silicate. Sampling of biogeochemical constituents was limited to outside of the Russian Exclusive Economic Zone (EEZ). The transects in the central Arctic Ocean span the Nansen, Amundsen, Canada, and Makarov Basins, separated by the Gakkel, Lomonosov, Alpha, and Mendeleev Ridges (Figure 2). Water for underway $O_2$/Ar and $pCO_2$ was taken from the ship's seawater intake near the bow of the ship at approximately 8 m below the waterline. A centrifugal pump (stainless steel/Teflon) with a fixed capacity of 4 $m^3\,h^{-1}$ supplied the water, of which a fraction was sampled.

### 3.2. Analytical Procedures

Biological oxygen supersaturation, $\Delta(O_2/Ar)$ (see section 3.3) [*Craig and Hayward*, 1987; *Emerson et al*., 1991], was continuously measured in seawater from the ship's seawater intake using Equilibrator Inlet Mass

Spectrometry [*Cassar et al*., 2009]. Briefly, seawater is pumped through a gas equilibrator, the headspace of which is connected to a quadrupole mass spectrometer (QMG 220 Prisma Plus 1–100 amu/Pfeiffer) for continuous elemental $O_2$/Ar ratio measurements. The ion current ratio was calibrated with air calibrations every 3 h. The instrument precision is ±0.3% or better [*Cassar et al*., 2009].

Nutrient concentrations were determined by a spectrophotometric autoanalyzer (Evolution III, Alliance instruments), using standard seawater methods. All nutrient samples were analyzed in duplicate with a precision of ±0.01 μM for phosphate, ±0.05 μM for nitrate and silicate in the concentration range from 0 to 20 μM, and ±0.1 μM for the higher concentrations. Calibration was performed (postcruise) on salinity and oxygen sensors from the CTD using discrete bottle samples, collected, and analyzed on board. The fluorescence measurements (Dr. Haardt fluorometer) were not calibrated against chlorophyll *a* [*Schauer*, 2012].

Samples of the carbonate system were collected in Pyrex® borosilicate bottles (250 mL) according to *Dickson et al*. [2007], without being poisoned with $HgCl_2$. Low productivity in Arctic waters combined with short-term sample storage (cold and dark) does not necessitate use of $HgCl_2$. DIC was determined using a coulometric titration method based on *Johnson et al*. [1987] with a modified Single Operator Multiparameter Metabolic Analyzer (SOMMA) system (coulometer type UIC 5012). The precision from replicate analyses during this cruise was ±4 μmol $kg^{-1}$, with the accuracy set by routine analysis of Certified Reference Materials (CRM, Batch #109) provided by A.G. Dickson, Scripps Institution of Oceanography, USA, with a correction factor ranging from 0.993 to 1.006 depending on station. TA was determined by open-cell potentiometric titration [*Haraldsson et al*., 1997] with a precision of ±1–2 μmol $kg^{-1}$. Here too, accuracy was ensured by routine analysis of CRM with a correction factor ranging from 0.996 to 1, depending on station. pH was determined spectrophotometrically (Agilent 8453) [*Clayton and Byrne*, 1993] on the total scale at 15°C ($pH^{15}_{tot}$). The perturbation of sample pH by addition of indicator solution (bulk meta-cresol purple sodium salt, Aldrich Lot #MKBC2604V) was corrected for using the method described by *Chierici et al*. [1999]. The overall precision from duplicate sample analysis was ±0.0004 units. The accuracy is mainly set by the accuracy in the temperature measurements and the determination of the equilibrium constants of the indicator and has been reported to be of the order of ±0.002 units [*Dickson*, 1993]. The carbonate system was overdetermined (DIC, TA, and pH) and was checked for internal consistency (Table S1 in the supporting information).

The partial pressure of carbon dioxide ($pCO_2$) was measured underway from the bow surface seawater intake by a permanently installed General Oceanics system (GO8050) with a nondispersive infrared $CO_2$ sensor (LI-COR® 7000). Because the measured $pCO_2$ is strongly dependent on temperature, the temperature difference between the water at the intake and in the equilibrium chamber of the GO system was recorded. Two thermosalinographs (Sea-Bird SBE4) in the bow (6 m) and the keel (11 m) thruster tunnels provided temperatures; note that the bow system was not employed during sea ice crossing [*Schauer*, 2012]. Calibration was performed several times per day against a series of four standard gases. The $pCO_2$ data were processed according to *Pierrot et al*. [2009] and Surface Ocean $CO_2$ Atlas (SOCAT)-approved methods [*Pfeil et al*., 2013]. The overall uncertainty was estimated to ±2 ppm.

### 3.3. NCP From Oxygen Mass Balance ($NCP_{O2/Ar}$)

Biologically mediated oxygen supersaturation in the surface ocean reflects the net metabolic balance between photosynthesis and respiration, i.e., NCP [*Reuer et al*., 2007]. The biological oxygen supersaturation was derived from underway $O_2$/Ar measurements where the physical processes affecting oxygen concentrations (e.g., temperature change, bubble entrainment, and mixing of waters with different temperatures) are accounted for by measuring argon (Ar), which has similar solubility properties as oxygen [*Craig and Hayward*, 1987]. The deviation of the $O_2$/Ar ratio from its saturation concentration ratio is defined as follows:

$$\Delta(O_2/Ar) = \left[\frac{([O_2]/[Ar])}{([O_2]/[Ar])_{sat}} - 1\right] \quad (1)$$

where $\Delta(O_2/Ar)$ represents the biological oxygen supersaturation [*Cassar et al*., 2011]. We assume that the summer mixed layer is at steady state with respect to $O_2$ in the surface layer such that $O_2$ efflux to the atmosphere balances NCP (see discussion below about errors associated with this approximation).

**Table 1.** End-Member Concentrations[a]

| End-Member | Seawater | River Runoff | Sea Ice Meltwater |
|---|---|---|---|
| Salinity | 34.86 | 0 | 4 |
| TA ($\mu$mol kg$^{-1}$) | 2297 | 1217 | 450 |
| DIC ($\mu$mol kg$^{-1}$) | 2165 | 1342 | 400 |

[a]The concentrations are used for estimates of the relative fractions of seawater, river runoff, sea ice meltwater, and preformed concentrations of DIC.

Daily $NCP_{O2/Ar}$ rates are estimated from the biological oxygen saturation, the oxygen concentration at saturation ($[O_2]_{sat}$), a gas transfer velocity ($k_{O_2}$), and a stoichiometric $O_2$:C ratio of 1.4 [*Laws*, 1991] according to

$$\mathrm{NCP}_{O_2/Ar}\ \left(\mathrm{mmol\ C\ m^{-2}\ d^{-1}}\right) \approx k_{O_2} \cdot [O_2]_{sat} \cdot \Delta(O_2/Ar) \cdot \frac{1}{O_2 : C} \quad (2)$$

The oxygen solubility is calculated from atmospheric pressure, temperature, and salinity [*Garcia and Gordon*, 1992]. The gas transfer velocity of oxygen (piston velocity) is estimated from the wind speed-dependent parameterization of *Wanninkhof* [1992] using wind components from the European Centre for Medium-Range Weather Forecasts Interim Re-analysis product (6 h, 0.75° resolution) and is weighted for wind history [*Reuer et al.*, 2007]. The estimated gas transfer velocity includes the effect of salinity and temperature on gas solubility. Linear [*Bates*, 2006; *Long et al.*, 2011] and nonlinear [*Loose et al.*, 2009] ice cover corrections are applied to the gas transfer velocity as a function of the fraction of open water, which for the latter case is given by

$$k_{O_2} = k_{100} \cdot f_{OW}{}^{0.4} \quad (3)$$

where $k_{100}$ is the piston velocity in open water. Ice concentration was interpolated along the cruise track from satellite data (AMSR-E 89 GHz until 4 October 2011, 6.25 km, available online at http://www.iup.physik.uni-bremen.de:8084/ssmis/) [*Spreen et al.*, 2008] synthesized from sea ice concentration maps from different days taking into account the changing sea ice cover during the cruise.

The daily $NCP_{O2/Ar}$ (mmol C m$^{-2}$ d$^{-1}$) estimates are multiplied by a growing season of 90 days [cf. *Codispoti et al.*, 2013] for comparison to the seasonal approaches (mol C m$^{-2}$) which are described in the subsequent sections.

### 3.4. NCP From Seasonal Drawdown of DIC ($NCP_{DIC}$ and $NCP_{pCO2}$)

Seasonal drawdown of DIC can be estimated by using estimates of preformed concentrations of dissolved inorganic matter as initial or winter concentrations, representing the concentrations of the waters entering the central Arctic Ocean [*Anderson et al.*, 2003; *Fransson et al.*, 2001]. Thus, these estimates reflect NCP integrated over the growing season up to the point of sampling. Preformed winter DIC concentrations are estimated from the fractions of seawater ($f_{sw}$), river runoff ($f_{rro}$), and sea ice meltwater ($f_{sim}$) using the corresponding end-member concentrations in the different source waters (Table 1):

$$\mathrm{DIC_{initial}} = (\mathrm{DIC_{sw}} \cdot f_{sw}) + (\mathrm{DIC_{rro}} \cdot f_{rro}) + (\mathrm{DIC_{sim}} \cdot f_{sim}) \quad (4)$$

The fractions $f_{sw}$, $f_{rro}$, and $f_{sim}$ are estimated according to the following three-component mass balance equations [*Anderson et al.*, 2004b; *Yamamoto-Kawai et al.*, 2005]:

$$1 = f_{sw} + f_{rro} + f_{sim} \quad (5)$$

$$S = S_{sw} \cdot f_{sw} + S_{sim} \cdot f_{sim} \quad (6)$$

$$\mathrm{TA} = \mathrm{TA_{sw}} \cdot f_{sw} + \mathrm{TA_{rro}} \cdot f_{rro} + \mathrm{TA_{sim}} \cdot f_{sim} \quad (7)$$

The river runoff fraction reflects the meteoric fraction within this study. The end-member concentrations from the different source waters used above are given in Table 1. These concentrations were derived from linear regression of all TA-S data deeper than 20 m (TA = 30.98S + 1217, $n = 1162$, $R^2 = 0.91$, $p < 0.001$) (Figure S1). The salinity of the seawater end-member of this regression line is 34.86, corresponding to a TA concentration of 2297 $\mu$mol kg$^{-1}$. The river runoff end-member was 1217 $\mu$mol kg$^{-1}$ and is assumed to be a valid mean concentration for the region of study, even if it is somewhat higher than the flow-weighted average from the major rivers entering the Arctic Ocean [*Cooper et al.*, 2008]. The sea ice meltwater is ascribed a salinity of 4 [*Anderson et al.*, 2004b; *Ekwurzel et al.*, 2001], making no distinction between multiyear ice and first-year ice. The TA concentration of sea ice meltwater is set to 450 $\mu$mol kg$^{-1}$ based on *Rysgaard et al.* [2012] and preliminary sack-hole measurements from ice station 218 ($n = 5$) during our cruise.

The DIC end-member concentrations for river runoff and sea ice meltwater are derived in a similar manner to TA (DIC = 23.64S + 1342, $n = 1162$, $R^2 = 0.64$, $p < 0.001$) (Figures S1 and S2). The difference between the preformed winter DIC concentrations and the measured discrete DIC concentrations integrated within the summer mixed layer is assumed to represent the seasonal biological drawdown of DIC, i.e., $NCP_{DIC}$:

$$NCP_{DIC}\left(\text{mmol C m}^{-2}\right) = \int_0^{MLD_S} \left(DIC_{initial} - DIC_{measured}\right) dz \tag{8}$$

Additionally, temporally high-resolution DIC concentrations were calculated with the widely used CO2SYS program [*van Heuven et al*., 2009] from underway $pCO_2$ measurements and total alkalinity, where the latter was obtained from a fixed salinity-total alkalinity relationship from the top 20 m (TA = 33.86S + 1108, $n = 113$, $R^2 = 0.75$, $p < 0.001$) (Figures S1 and S2), using the stoichiometric dissociation constants of carbonic acid ($K_1^*$ and $K_2^*$) and bisulfate ($K_{HSO4}^*$) given by *Roy et al*. [1993] and *Dickson* [1990], respectively. Underway $NCP_{pCO2}$ estimates are derived from these calculated DIC concentrations and the preformed DIC concentrations within the summer mixed layer, similar to the approach for the discrete $NCP_{DIC}$ (equation (8)). The summer mixed layer depth ($MLD_s$) was estimated from CTD profiles and is defined as the depth at which the density increases from its surface value to 20% of the difference between 100 m and surface values [*Rutgers van der Loeff et al*., 2014; *Shaw et al*., 2009]. We assume an average $MLD_s$ of 21 m for all stations.

### 3.5. NCP From Seasonal Drawdown of Nutrients and DIC ($NCP_{nuts}$)

Biological seasonal drawdown of nutrients can be estimated from the difference between summer concentrations in the surface mixed layer and winter surface water concentrations, either by using seasonal data [*Mathis et al*., 2010; *Shadwick et al*., 2011] or by inferring winter concentrations from summer profiles [*Jennings et al*., 1984]. Data of winter and spring concentrations are scarce in the central Arctic Ocean [cf. *Codispoti et al*., 2013]. Therefore, following *Rudels et al*. [1996], the temperature minimum located below the halocline, inferred from summer CTD profiles, is assumed to indicate the depth of winter convection during the previous winter ($MLD_w$). If no obvious temperature minimum is found, salinity profiles are included in the analysis since a steepening of the salinity gradient often begins directly below the temperature minimum.

We assume the temperature minimum to be remnant of the mixed layer formed during the previous winter and thus represent the properties of the winter mixed layer. Nutrients are assumed to have similar conservative properties as temperature and salinity such that surface layer depletions in nutrients are only ascribed to biological drawdown. Vertical and lateral mixing in the surface layer and the temperature minimum are assumed to be small. Thus, the water column down to the base of the winter mixed layer is assumed to be affected by spatially homogeneous biogeochemical and physical processes only and also that realistic temporal scales (e.g., growing season) are considered, over which the depletion occurs [*Hoppema et al*., 2000, 2007; *Jennings et al*., 1984]. This approach has previously been successfully applied in the Southern Ocean [e.g., *Hoppema et al*., 2000, 2007; *Ishii et al*., 2002], where similar or equal nutrient concentrations were found at the temperature minima during summer compared to the winter water surface layer [*Pondaven et al*., 2000; *Rubin et al*., 1998]. The nutrient concentrations at the temperature minimum are acquired through linear interpolation between nearest neighboring sampling depths.

Two sets of $NCP_{nuts}$ estimates are derived from vertically integrated deficits [*Hoppema et al*., 2000] of total inorganic nitrogen ($[NO_3^-] + [NO_2^-] + [NH_4^+]$) (N), phosphate (P), and DIC (C); (i) over the summer mixed layer for comparison to the previously described approaches and (ii) over the winter mixed layer, according to

$$NCP_X\left(\text{mmol C m}^{-2}\right) = \int_0^{MLD_s,\ MLD_w} \left(\left(X_{initial} - X_{measured}\right)\right) dz \cdot \left(R_{C/X}\right) \tag{9}$$

where $X$ denotes the nutrient (N, P, or C) and $R_{C/X}$ denotes the carbon to nutrient stoichiometric ratio. "Initial" refers to the nutrient concentration of the layer at the beginning of the growing season (i.e., the nutrient concentration obtained at the depth of the temperature minimum), and "measured" refers to the profile samples. As the dilution by sea ice melt and river runoff is assumed to have a negligible impact on nutrient concentrations, this approach does not add any unknown errors compared to the previous approach (section 3.4). For DIC and TA, this dilution may have a major effect relative to the impact by NCP.

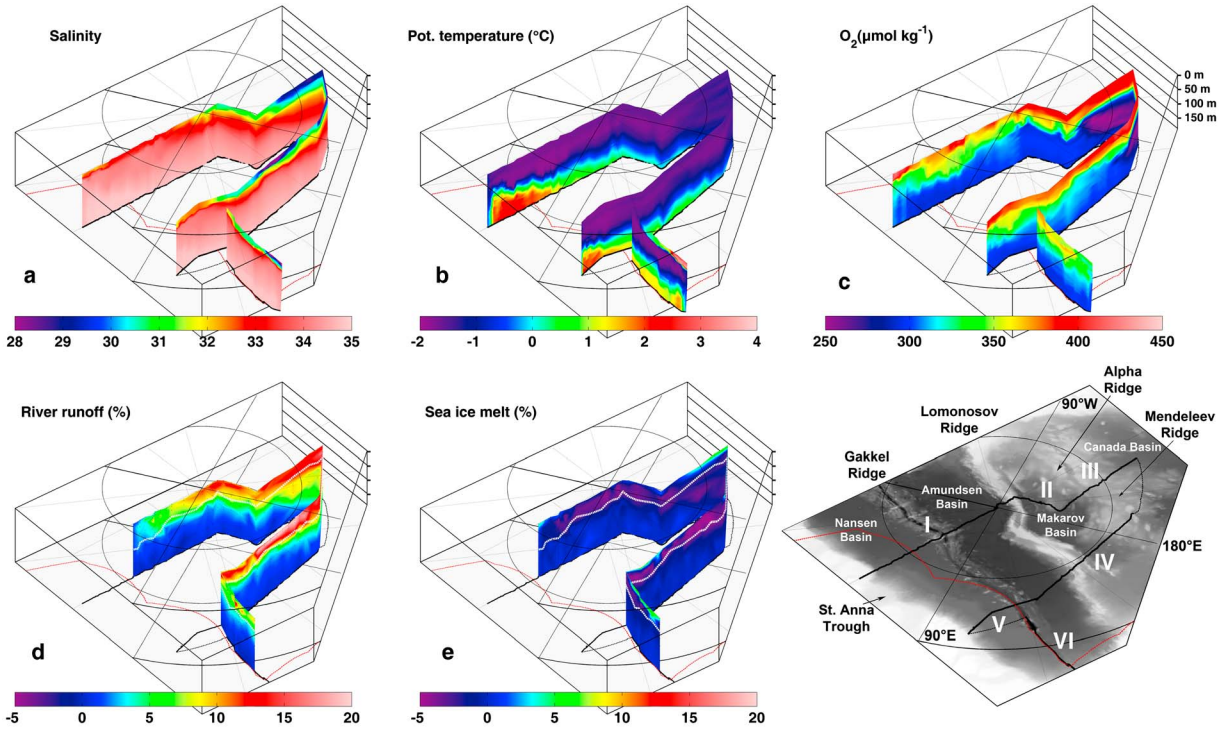


**Figure 3.** Sections of the upper 150 m of (a) salinity, (b) potential temperature, (c) dissolved oxygen, (d) fraction of river runoff, and (e) fraction of sea ice meltwater together with the cruise track (black line) overlaid on the bathymetry. The solid black line represents sections of CTD sampling of salinity, temperature, and oxygen, while the thin dotted lines are transits. Note that river runoff and sea ice melt rely on total alkalinity data which are only available for stations outside the Russian EEZ, indicated by the red line (see also Figure 2). The white lines in these figures indicate the depth of the winter mixed layer ($MLD_w$). Roman numerals indicate sections referred to in the text.

Note that $NCP_C$ denotes the vertically integrated deficits of DIC in this approach, not to be confused with $NCP_{DIC}$ (see section 3.4). DIC was normalized according to [*Friis et al.*, 2003]:

$$DIC_{norm} = \frac{(DIC_{measured} - DIC_{rro})}{S_{measured}} S_{mean} + DIC_{rro} \quad (10)$$

where $DIC_{rro}$ is the river runoff end-member concentration (Table 1). The nutrient deficits were converted to carbon deficit equivalents through the Redfield stoichiometric ratio of 106C:16N:1P [*Redfield et al.*, 1963]. The calculated deficits represent the time-integrated changes of the summer and winter surface layers from the end of the winter period to the point of sampling.

## 4. Results

### 4.1. Hydrographic Structure

All surface waters, except along the transect closest towards the Laptev Sea (Figure 3, Section VI), were cold and close to the freezing point with a strong thermocline (~100–200 m) separating them from the underlying warmer water of Atlantic origin (Figure 3). The temperature of the Atlantic layer decreased from the Nansen Basin toward the Canada Basin (Section I) as did the salinity in the upper surface layers. Low-salinity (~28) surface water was observed in the Makarov Basin (Section III) and the crossing of the Amundsen Basin (Section IV) closest to the Laptev Sea (Figure 3a), indicating a strong flow of riverine-derived shelf water from the Laptev Sea region. Sea ice meltwater contributed substantially to the freshwater at the surface of the section along the Gakkel Ridge, heading toward the Laptev Sea (Section VI) and added about an equal amount (i.e., 5% to 10%) as the river runoff (Figures 3d and 3e). Over the Alpha-Mendeleev Ridge (Sections II–IV), a fair fraction (up to 5%) of sea ice melt was observed. However, in this region the river runoff contribution was very high (more than 15%), making the sea ice melt fraction relatively smaller. A slight signature of negative sea ice meltwater, i.e., a signature of brine from sea ice formation, was seen below the layer of sea ice melt (Figure 3e).

Dissolved oxygen concentrations exhibited supersaturated levels throughout the summer mixed layer (Figure 3c), except for a slight undersaturation in the Amundsen Basin (Section I) and toward the Laptev Sea (Section VI). The vertical structure of dissolved oxygen reflected the different water masses in the different basins, and an obvious subsurface minimum centered at round 100 m was observed in the Canada Basin (Section III) below the depth of the winter mixed layer.

The average $MLD_w$ was 63 ± 20 m in the Nansen Basin, 57 ± 14 m in the Amundsen Basin, and 53 ± 7 m in the Makarov Basin (Sections I and II). Stations above ridges and close to the slope were not included in these estimates. A shallow $MLD_w$ (40 m) was found over the shelf north of Franz Josef Land (Figure 3), followed by a drastic drop (90 m) offshore from the continental slope which was again seen offshore north of Severnaya Zemlya (Section V). The $MLD_w$ was variable throughout the Nansen Basin (60–100 m) with greater depths in the central basin, followed by shallower $MLD_w$ in the Amundsen Basin and even shallower ones in the Canada Basin (40 m). Slightly deeper $MLD_w$ was found in the Makarov Basin, peaking (30 m) along the eastern transect over the Lomonosov Ridge (Section IV) and then returning to similar depths as those found along the central transects in the Amundsen and Nansen Basins. During summer, the mixed layer is significantly shallower and the average $MLD_s$ was 21.5 ± 4.2 m for all stations occupied during the cruise (Stations 201–280).

### 4.2. Sea Ice Conditions

The sea ice conditions in late summer 2011 were recently described by *Nicolaus et al*. [2012]. Briefly, the sea ice extent was 5.5 million $km^2$ with a mean sea ice concentration of 63% with little or no snow cover in general. First-year ice (FYI) dominated the eastern Eurasian and Makarov Basins, whereas multi-year ice (MYI) dominated the central Amundsen Basin and the western subregions. During the cruise there was extensive melt pond coverage (Figure 5) for both FYI (42 ± 10%) and MYI (23 ± 13%). Ice stations occupied prior to reaching 90°N had open melt ponds, while surface freezing was observed thereafter.

### 4.3. Nutrients and Fluorescence

The nutrient distributions were largely determined by water masses and the general ocean circulation, with imprints of biogeochemical processes. These were dominated by primary production in the surface water where the concentrations were very low (Figures 4a–4c). Two apparent peaks in fluorescence were observed at the shelf break north of Franz Josef Land (Section I) and south of the Gakkel Ridge in the Nansen Basin (Section V). However, generally, the fluorescence intensity was not very high and mostly found in the top ~20 m (Figure 4f). This was shallower than the nitrate and even more than the phosphate drawdown depth, indicating a low supply of nutrients in this region.

Another feature in the nutrient sections was the subsurface maximum in the area closest to the Canada Basin (Section III) which also coincided with the oxygen minimum (Figure 3c). The maximum was most obvious in silicate and phosphate (Figures 4b and 4c) but could to some extent also be observed in nitrate (Figure 4a).

### 4.4. Carbonate System

The DIC and TA distributions along the cruise track largely reflected the salinity as the impact by biogeochemical processes was relatively small (Figures 4d and 4e). There was a small drawdown of DIC in the surface water of the Nansen Basin in the regions with the highest fluorescence. The largest signature in $pH_{tot}^{15}$ and $pCO_2$ (calculated from TA, $pH_{tot}^{15}$, and in situ temperature) was found in the subsurface waters at around 100 m depth (Figures 4g and 4h), with the magnitude highest toward the Canada Basin (Section V). This coincided with high nutrient concentrations of the upper halocline waters consistent with organic matter remineralization as described by, e.g., *Jones and Anderson* [1986].

### 4.5. Surface Water $pCO_2$

Underway surface $pCO_2$ was consistently undersaturated with respect to the atmosphere (~390 μatm) in the central Arctic Ocean (Figure 5). The lowest values coincided with the ice edge at the shelf breaks north of Franz Josef Land (<150 μatm) and Severnaya Zemlya (190 μatm). Through the Nansen and Amundsen Basins along 60°E (Section I), $pCO_2$ increased as the salinity decreased with only a slight increase in temperature, reaching a maximum at 90°N (350 μatm). In the Canada Basin (Section III), $pCO_2$ decreased until reaching the Makarov Basin and the Lomonosov Ridge, where it increased while returning back to the Amundsen Basin (Section IV).

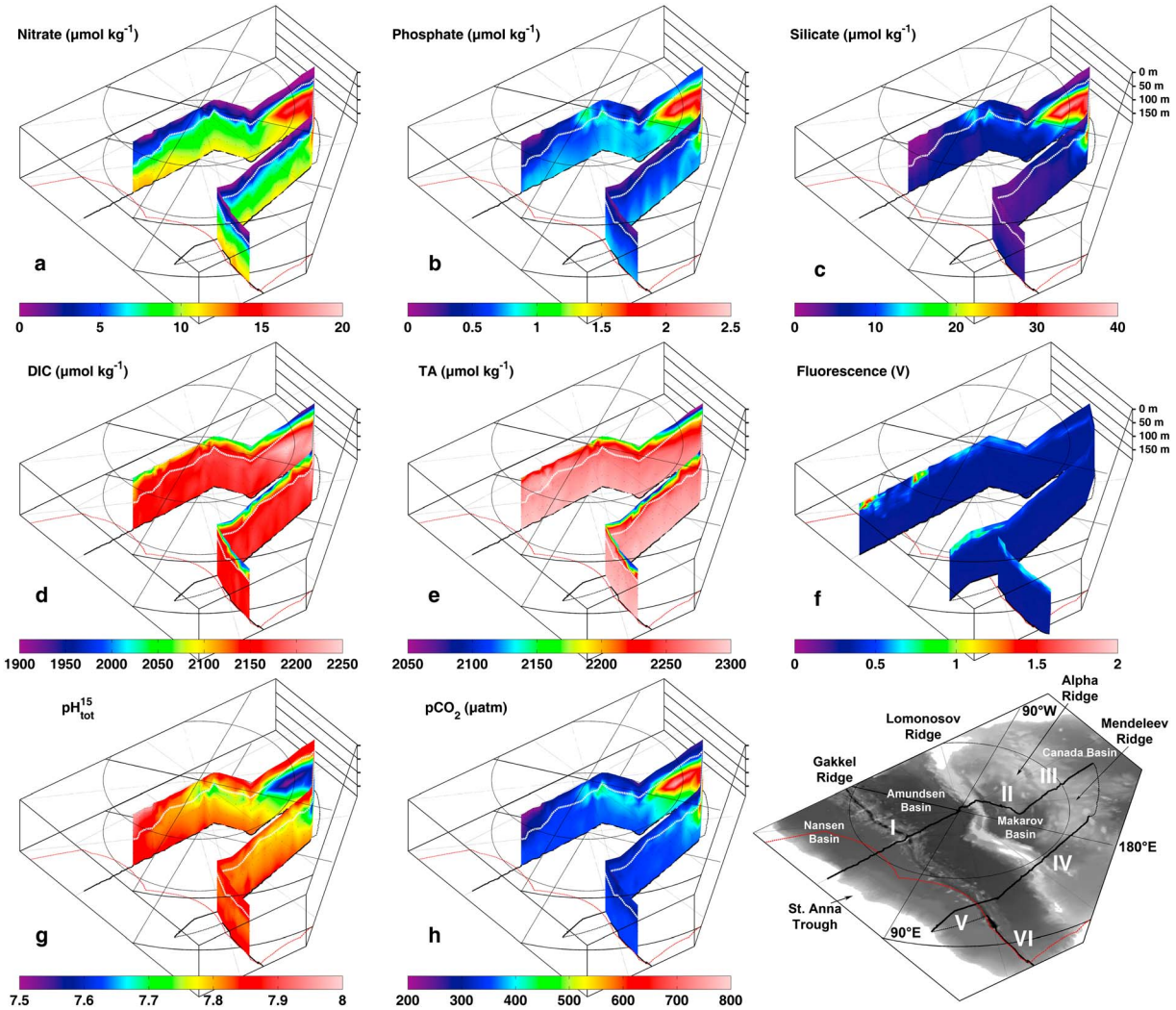


**Figure 4.** Sections of the upper 150 m of (a) nitrate, (b) phosphate, (c) silicate, (d) DIC, (e) TA, (f) fluorescence, (g) $pH^{15}_{tot}$, (h) $pCO_2$, and the cruise track (refer to Figure 2 for details).

### 4.6. Surface Water $\Delta(O_2/Ar)$

The biological oxygen supersaturation mirrored the $pCO_2$ distribution (Figure 5) with a high degree of negative correlation ($n = 1739$, $R^2 = 0.71$, $p < 0.001$), reaching a maximum supersaturation of 21% along the shelf break where the $pCO_2$ minimum was observed. This is consistent with the notion that the $pCO_2$ signal is clearly controlled by biological processes. At, or just south of, the Gakkel Ridge (Section I) there was another peak in $\Delta(O_2/Ar)$ reaching 13%, which was of similar magnitude as the peaks over the Mendeleev Ridge (10%) and north of Severnaya Zemlya (13%). The only biological oxygen undersaturation (−1.7%) was observed close to 90°N, implying that most of the surface waters along the transects were net autotrophic over the residence time of oxygen under the ice.

### 4.7. Estimates of NCP

Late summer NCP (mol C $m^{-2}$) in the surface mixed layer in the central Arctic Ocean (Figure 5) was estimated by our four different approaches. Until leaving the Russian EEZ north of 85°N (13 August), only underway $NCP_{O2/Ar}$ estimates were available. Underway $NCP_{pCO2}$ was assumed to be only representative where it could be constrained by discrete $NCP_{DIC}$ estimates. The range of $NCP_{O2/Ar}$, indicated by the transparent envelope in Figure 5, is a result of linear (lower limit) and nonlinear (upper limit) ice correction of the gas transfer velocity. The given estimates are presented as the average of the upper and lower limits.

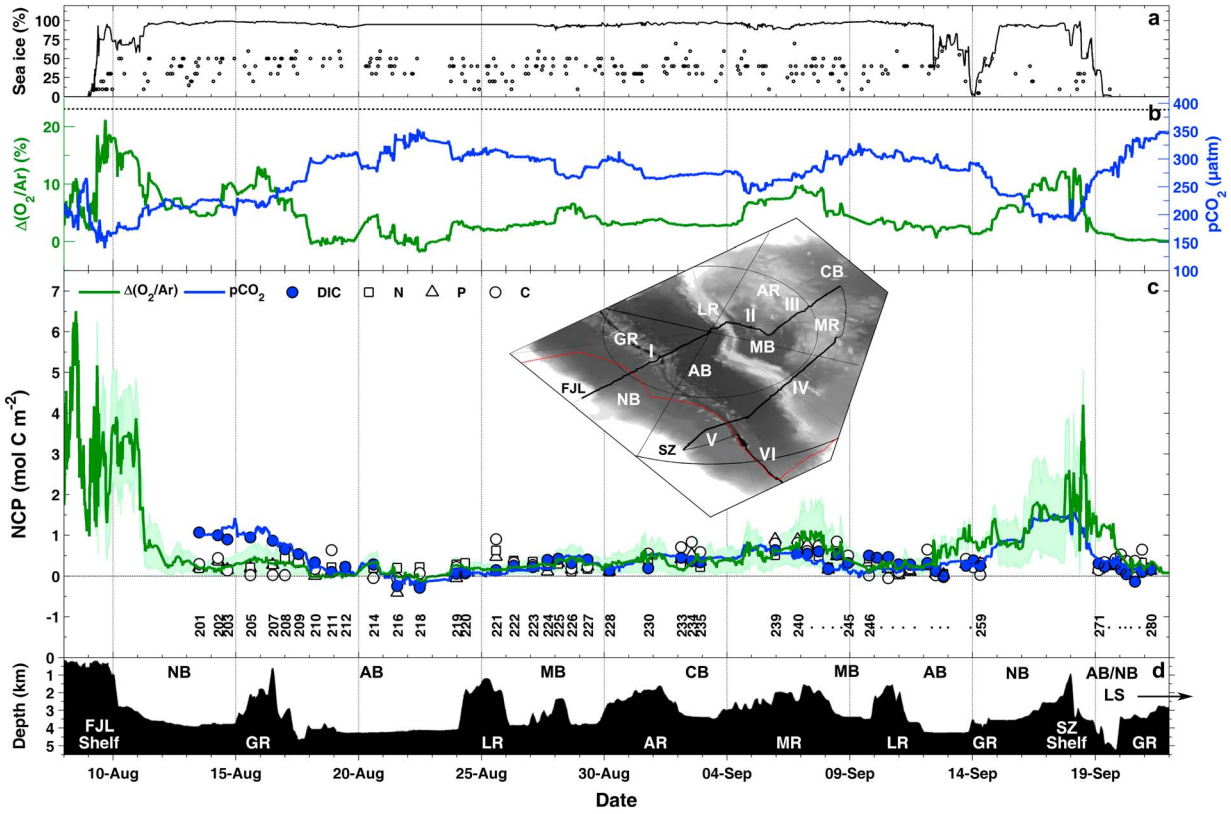


**Figure 5.** (a) Ice concentration (line) interpolated from satellite data along the cruise track and bridge observations of melt pond coverage (dots). (b) Surface $pCO_2$ and biological oxygen supersaturation, $\Delta(O_2/Ar)$, along the cruise. The atmospheric $pCO_2$ is indicated by the dashed line. (c) Late summer NCP (mol C $m^{-2}$) estimated by the different approaches as denoted in the figure. CTD stations are denoted by their station numbers. (d and inset map) The cruise track and bathymetric features; FJL, Shelf north of Franz Josef Land; GR, Gakkel Ridge; LR, Lomonosov Ridge; AR, Alpha Ridge; MR, Mendeleev Ridge; SZ, Shelf north of Severnaya Zemlya. See also Figure 2 for basin abbreviations and for an overview of the cruise track.

Generally, the overall pattern showed moderate to high NCP (2 to 6 mol C $m^{-2}$) in the marginal ice zone north of Franz Josef Land. Northward into the Nansen Basin (Section I) along 60°E, the NCP decreased drastically (0 to 0.5 mol C $m^{-2}$). The lowest values were found in the Amundsen Basin, where even negative values (–0.4 to 0.6 mol C $m^{-2}$) were observed close to 90°N (22 August), indicating temporary heterotrophy or vertical mixing of $O_2$ depleted waters. Slightly higher NCP (0 to 1 mol C $m^{-2}$) were found over the Lomonosov Ridge and into the Canada Basin and farther over the Alpha Ridge. A wide peak (up to 1 mol C $m^{-2}$) was observed in the Makarov Basin over the Mendeleev Ridge (Section IV), and then lower values (0 to 0.5 mol C $m^{-2}$) decreasing over the Lomonosov Ridge down to the values in the Amundsen Basin. A similar NCP as in the central basin was found in the eastern Nansen Basin, and again a peak (up to 3 mol C $m^{-2}$) at the ice edge close to the shelf north of Severnaya Zemlya. Low values similar to those found in the Nansen Basin were seen following the extension of the Gakkel Ridge toward the Laptev Sea (Section VI).

## 5. Discussion

The NCP in the central Arctic Ocean estimated by our different approaches ultimately depends on the supply of nutrients to the photic zone, as well as the availability of light. These two parameters are largely constrained by the hydrographic structure and by the sea ice conditions. Generally, the availability of light sets the onset of the growing season, and the nutrient supply the magnitude and duration of the primary production as nutrients are utilized until depletion during the growing season [*Carmack et al.*, 2006].

The Nansen Basin is influenced by inflowing Atlantic Water, providing nutrients to the subsurface layers that may feed the upper layers during winter convection, which reaches deeper in the Nansen Basin compared to the other deep basins. The nutrient maximum in the Makarov and Canadian Basins is the well-known signature of the upper halocline with its ultimate source being Pacific Water, which enters the central Arctic

**Table 2.** Mean Differences and Standard Deviations of NCP Estimates[a]

| Parameter | Mean | SD | Slope | $R^2$ | $n$ |
|---|---|---|---|---|---|
| $NCP_{O2/Ar}$[b] | −0.170 | ± 0.18 | 1.03 | 0.62 | 861 |
| $NCP_N$ | 0.026 | ± 0.18 | 0.30 | 0.19 | 46 |
| $NCP_P$ | −0.001 | ± 0.17 | 0.90 | 0.53 | 46 |
| $NCP_C$ | 0.090 | ± 0.27 | 0.53 | 0.17 | 46 |

[a]Underway $NCP_{O2/Ar}$ versus $NCP_{pCO2}$ and discrete $NCP_{nuts}$ versus $NCP_{DIC}$, in mol C $m^{-2}$. Slopes and $R^2$ of the resulting linear regressions are given.

[b]Note that the underway estimates are only between 18 August and 12 September due to the apparent mismatch in Figure 5 prior to and after these dates.

through the Chukchi and East Siberian Seas via Bering Strait [*Anderson et al*., 2010; *Weingartner et al*., 2005]. Pacific Water also feeds the western Amundsen Basin. As a result of biological consumption of nutrients, strong stratification, shallow winter convection, and a long transit time, these waters are generally depleted in nutrients and a low NCP is expected. This is similar to the conditions in the eastern Nansen Basin due to long advective timescales of Atlantic Water via the Barents Sea and Nansen Basin. In contrast, in the eastern Amundsen and Makarov Basins, shelf bottom waters with high nutrient concentrations are supplied to the subsurface waters by the continental shelf pump on a shorter timescale [*Popova et al*., 2013].

### 5.1. Comparison of Approaches

In the central and eastern Nansen Basin, diverging estimates (up to 1 mol C $m^{-2}$) were observed for the $NCP_{O2/Ar}$ and $NCP_{pCO2}$. Excluding the apparent discrepancies in the central and eastern Nansen Basin between 18 August and 12 September (Figure 5), there was a fairly high degree of correlation ($n = 861$, $R^2 = 0.62$, $p < 0.001$) between the $NCP_{O2/Ar}$ and $NCP_{pCO2}$ estimates (Table 2). Estimates of discrete $NCP_{DIC}$ and $NCP_{nuts}$ agree with the general pattern of the underway estimates but with a large scatter, typically within ±0.5 mol C $m^{-2}$. $NCP_{DIC}$ indicates how well the $NCP_{pCO2}$ approach is performing since they are derived from a similar approach. The former relies on discrete measurements, and the latter on underway $pCO_2$ measurements and a fixed TA-S relationship, assumed to be valid for the entire region of our study. They agree fairly well, acknowledging diverging estimates particularly in the Makarov Basin and toward the Laptev Sea.

In the Nansen Basin, $NCP_{nuts}$ followed the general pattern of $NCP_{O2/Ar}$, with the exception of $NCP_C$ which was close to zero over the Gakkel Ridge. The largest discrepancies in $NCP_{nuts}$ with respect to $NCP_{DIC}$ were found in the Nansen, Amundsen, and Makarov Basins. $NCP_{nuts}$ were conspicuously divergent at stations 211, 216, and 221. $NCP_P$ has the smallest mean discrepancy compared to $NCP_{DIC}$ (Table 2).

It should be noted that the $NCP_{O2/Ar}$ estimates are presented as the mean of estimates of different sea ice corrections of the gas transfer velocity. The mean of the weighted gas transfer velocity in open water was 2.4 ± 0.9 m $d^{-1}$. Within the sea ice cover it was 0.09 ± 0.04 m $d^{-1}$ and 0.5 ± 0.2 m $d^{-1}$ for the linear and nonlinear sea ice correction, respectively, with the mean of 0.3 m $d^{-1}$. A recent study by *Rutgers van der Loeff et al*. [2014] suggests that gas exchange does not exceed expectations based on a linear scaling to percent sea ice cover, estimated from $^{222}Rn$ measurements during the cruise. Although little can be said about the residence time of $O_2$ as a result of poorly constrained gas exchange, it is expected to be much greater than in open water. Since sea ice seriously impairs gas exchange, $O_2$ might be expected to behave more like a nutrient with no gas exchange, especially in the beginning of the growing season prior to summer sea ice melt. In the surface ocean, the residence time of oxygen is approximately 1–2 weeks. Assuming the mean piston velocity of 0.3 m $d^{-1}$ under the ice, and an average mixed layer depth of 21 m, the residence time of $O_2$ would be approximately 70 days, which is similar to the residence time of nutrients, and may partially explain the general overall agreement between the various methods.

### 5.2. Comparison to Other Estimates

Our late summer seasonal estimates of NCP (g C $m^{-2}$) are comparable to the range of mean rates given by *Codispoti et al*. [2013] for the corresponding basins and subregions (Table 3) considering the overall uncertainty, acknowledging possible differences in both spatial and temporal resolution, as well as in methodology. The recent synthesis by these authors of nitrate- and phosphate-based estimates of the seasonal NCP, assuming a

**Table 3.** Seasonal NCP Estimates (g C $m^{-2}$)[a]

| Subregion/Basin[b] | $NCP_{O2/Ar}$ ($MLD_S$) | $NCP_{pCO2;DIC}$ ($MLD_S$) | $NCP_{nuts}$ ($MLD_S$) | $NCP_{nuts}$ ($MLD_W$) | *Codispoti et al.* [2013] |
|---|---|---|---|---|---|
| Barents (Bering) Sea | | | | | 30–50 |
| Marginal Ice Zone | 15–90 | - | - | - | (50–200) |
| Eurasian Basin | | | | | 5–25 |
| Nansen Basin | 5–10 | 10–15 | 2–5 | 5–25 | |
| Amundsen Basin | −2–5 | −5–10 | −5–8 | −5–22 | |
| Amerasian Basin | | | | | 0.5–5 |
| Canada Basin | 3–10 | 2–8 | 2–10 | 5–20 | |
| Makarov Basin | 0–5 | 0–5 | 0–10 | 0–20 | |
| ESS + Laptev Northern | | | | | 3–15 |
| Mendeleev Ridge | 3–10 | 0–10 | 5–10 | 10–30 | |
| ESS + Laptev Southern | | | | | 5–30 |
| Amundsen/Nansen Eastern | 0–40 | 0–15 | 0–10 | 0–15 | |

[a]Range of seasonal NCP estimates in the summer and winter mixed layers compared to the range given by *Codispoti et al.* [2013] for corresponding basins and subregions. Seasonal estimates $NCP_{O2/Ar}$ assuming a growing season of 90 days.
[b]Subregions as defined in *Codispoti et al.* [2013] compared to the corresponding regions occupied during ARK XXVI/3. East Siberian Sea is denoted as ESS.

growing season of 86 days, suggests moderate mean rates of NCP (10–15 g C $m^{-2}$) in the Eurasian Basin and low rates (~10 g C $m^{-2}$) in the Laptev and northern Chukchi subregions. Even lower rates (~1–5 g C $m^{-2}$) are estimated for the Northern Beaufort and Amerasian Basin subregions, which is comparable to previous estimates of export production (~0.5 g C $m^{-2}$ $yr^{-1}$) from phosphate deficits in the central Arctic Ocean [*Anderson et al.*, 2003]. Further, *Codispoti et al.* [2013] report high rates (~30–40 g C $m^{-2}$) in the Nordic and Barents Seas, and very high rates in the Bering (50–200 g C $m^{-2}$) and southern Chukchi (40–120 g C $m^{-2}$) subregions.

It should be noted that since the $NCP_{O2/Ar}$ and $NCP_{pCO2}$ approaches are based on underway surface measurements and thus only applicable in the uppermost layer, NCP estimates from the various approaches are compared over the depth of the summer mixed layer. This will represent a fraction of the total, since NCP is also expected below the surface layer. Nutrient deficits are, however, vertically integrated over both the summer and winter mixed layer, the latter representing the total NCP (Tables 3 and S2). The integration depth and time interval used by *Codispoti et al.* [2013] were chosen so that the highest yields of NCP were obtained based on changes in nitrate and phosphate. In the central Arctic Ocean this depth was at least 50 m and did not exceed 100 m, similar to our estimated winter mixed layer depths.

Our high $NCP_{O2/Ar}$ (up to 6 mol C $m^{-2}$) in the marginal sea ice zone are of the same order of magnitude as estimates from the productive Bering Sea region based on the drawdown of DIC and nutrients [*Cross et al.*, 2012; *Mathis et al.*, 2010], as well as mean NCP rates (88 ± 15 mmol C $m^{-2}$ $d^{-1}$) estimated for the coastal region of the Gulf of Alaska from $\Delta(O_2/Ar)$ measurements [*Palevsky et al.*, 2013]. The high rates are also comparable to previous estimates of new production associated with ice-edge phytoplankton blooms [e.g., *Mundy et al.*, 2009] which are significant features of Arctic primary production [*Sakshaug*, 2004] and occur in all seasonally ice-covered areas from spring to late summer [*Perrette et al.*, 2011, and references therein]. The blooms generally follow the receding and melting ice edge which provides light and nutrients but are highly variable in production both spatially and temporally.

Another possible spot of enhanced primary productivity was found by the biological oxygen supersaturation over a shallow seamount (~600 m) at the Gakkel Ridge in the Nansen Basin (station 207). A closer inspection of the individual data profiles (Figure S3) at adjacent stations suggests a horizontal eddy-like feature that weakens the halocline and thus allows nutrients to be mixed upward into the photic zone. Local mixing events such as cyclonic and anticyclonic eddies can play an important role for the local productivity, especially in the deep basins, bringing up nutrients into the photic zone [*Timmermans et al.*, 2008; *Tremblay et al.*, 2008]. Topographically induced mixing has previously been shown to be of importance at lower latitudes [*Lueck and Mudge*, 1997], in the Weddell Sea around Maud Rise [*Muench et al.*, 2001], and to some extent also in the Arctic

Ocean [*Rainville and Winsor*, 2008]. The corresponding peak in $NCP_{O2/Ar}$ is less apparent than the $\Delta(O_2/Ar)$ peak as a result of hampered gas exchange due to sea ice cover. Estimates of $NCP_{nuts}$ are even lower, which may be due to different integration timescales. While the nutrient approach integrates over the growing season, the $O_2$/Ar approach integrates over the residence time of $O_2$ in the mixed layer.

### 5.3. Assumptions and Caveats

The approaches presented harbor common and independent assumptions, limitations, and uncertainties. It is impossible to estimate an absolute uncertainty for each approach. It should be noted that the overall uncertainty can be more than 100%, exemplified by the $NCP_{O2/Ar}$ estimates, which depend on the ice-correction method of the gas transfer velocity. Although the agreement between methods is encouraging, we cannot rule out common biases.

#### 5.3.1. Stoichiometry and Growing Season

Varying elemental stoichiometry may be a significant source of uncertainty. The NCP estimates from the different proxies are interrelated through the nutrient stoichiometry, assuming Redfield C:N:P (106:16:1) ratios. Several studies suggest higher C:N:P ratios [e.g., *Anderson and Sarmiento*, 1994; *Sterner et al*., 2008]. Recently, *Frigstad et al*. [2014] evaluated the applicability of the Redfield C:N ratio in the Arctic Ocean and pan-Arctic shelves based on observations of particulate organic carbon (POC) and nitrogen (PON). They found significantly higher ratios on a regional basis (7.9 on average), except for the central Arctic Ocean (6.6), Chukchi (6.4), and East Siberian (6.5) Seas. In contrast, *Tamelander et al*. [2012] found an average C:N ratio of 9.7 for the central deep Arctic Ocean based on exported POC:PON ratios, implying up to 40% higher carbon export compared to Redfield-based estimates. However, although Redfield uptake ratios can vary significantly over short time scales, we assume a constant Redfield ratio to be approximately correct when averaged over the growing season [*Codispoti et al*., 2013; *Hoppema and Goeyens*, 1999].

The assumption of a growing season of 90 days for the $NCP_{O2/Ar}$ estimates is somewhat arbitrary, ranging from 60 to 120 days in the literature [*Anderson et al*., 2003; *Codispoti et al*., 2013; *Sakshaug*, 2004; *Wassmann et al*., 2006]. Assuming a different growing season length leads to a proportional change in the seasonal $NCP_{O2/Ar}$ estimates.

#### 5.3.2. Freshwater and Variability

Both the $NCP_{DIC}$ and $NCP_{pCO2}$ rely on linear TA-S relationships. Large variable contributions of river runoff and sea ice meltwater in the summer mixed layer result in significant uncertainties. The difference between the measured TA in the summer mixed layer and that computed from salinity at the same stations using the linear relationship gives a mean of 4 $\mu$mol kg$^{-1}$ with a standard deviation of 23 $\mu$mol kg$^{-1}$. The largest discrepancies were found in the Canada Basin and the sections toward the Laptev Sea, where the linear relationship overestimates TA by ~30 $\mu$mol kg$^{-1}$, whereas in the Makarov Basin it underestimates TA by 30 to 60 $\mu$mol kg$^{-1}$ (Figure S2). This procedure may underestimate the runoff concentration as a result of DIC consumption by primary production. However, the resulting computed $pCO_2$ is high (~1700 $\mu$atm) and in the same range as reported for the Lena River with around 600 $\mu$atm in summer and up to 5800 $\mu$atm in winter [*Semiletov et al*., 2011], indicating that an underestimation is unlikely.

Nonconservative variability in TA concentrations can result from carbonate mineral precipitation or dissolution [*Cross et al*., 2013]. Calcifying plankton has been reported in the Barents and Bering Seas, but up to now not in any substantial amount within the central Arctic Ocean, making this a minor source of uncertainty for the $NCP_{DIC}$ estimates. In addition, $CaCO_3$ crystals (e.g., ikaite) have been observed to precipitate in the brine channels during sea ice formation and can be retained within the sea ice matrix during brine release [*Fransson et al*., 2013; *Rysgaard et al*., 2007]. This leads to a deficit in TA in the brine and elevated TA in the sea ice melt relative to its salinity. This process has been observed in local studies but has not yet been shown to make a large-scale impact. In addition, ikaite was not observed in the sea ice during the cruise (G. Dieckmann, personal communication, 2011). Estimates of the freshwater fractions using $\delta^{18}O$ have shown somewhat different results than the ones using TA, but they do not vary substantially [*Yamamoto-Kawai et al*., 2005], supporting the use of TA for this purpose. Different studies use different definitions of the seawater end-member as well as site-dependent source water concentrations, only allowing for relative comparisons of general distribution patterns between studies [*Lansard et al*., 2012].

The surface $pCO_2$ of the central Arctic Ocean is generally undersaturated with respect to the atmosphere. The state of undersaturation is set by increased gas solubility from cooling of the inflowing warm surface waters.

Additionally, intense primary productivity over the inflowing seasonally sea ice-free marginal seas and the mitigating effect of the sea ice cover on the air-sea exchange promote undersaturation in the surface waters [*Anderson et al*., 2010; *Bates and Mathis*, 2009; *Fransson et al*., 2009]. Contributions of air-sea flux of $CO_2$ to NCP were explicitly excluded in the analysis, because they are estimated to be less than 5% assuming open water conditions (and likely less under sea ice), which is similar to other estimates [*Hoppema and Goeyens*, 1999; *Mathis et al*., 2010]. Temperature normalization of $pCO_2$ [*Takahashi et al*., 2002, 2009] has only a small effect on the estimated NCP, less than 0.005 mol C $m^{-2}$ along the ice-covered transects and less than 0.05 mol C $m^{-2}$ along the last transect toward the Laptev Sea, where the NCP is low. Considering the overall uncertainty and the small changes, temperature normalization of $pCO_2$ was neglected in the analysis. However, we cannot rule out $pCO_2$ undersaturation associated with advection of warmer waters into the ice-covered regions (i.e., advection faster than gas exchange equilibrium time).

#### 5.3.3. Nutrient Deficits and Temperature Minimum

The nutrient concentrations at the temperature minimum are acquired through linear interpolation between nearest neighboring sampling depths; however, the vertical resolution is often rather low (typically, surface 10, 25, 50, 75, 100, and 150 m). The uncertainty in the depth of the winter mixed layer from the determination of the temperature minimum is generally ±5 m. Data from ice-tethered profilers [*Krishfield et al*., 2008] in the Canada Basin suggests that the maintenance of the winter convection (and the vertical mixing of nutrients) ends in May. However, the remnant of the winter mixed layer is conserved below the summer halocline, approximately at the depth of maximum winter convection until the end of summer, i.e., the time of our observations (August/September) [*Korhonen et al*., 2013].

Ideally, at the depth of the temperature minimum, the temperature should be equal or close to the freezing point if it is to represent a true remnant of the preceding winter surface layer. In the deep basins, the temperature minima differ from the freezing point temperatures by an average of 0.12 ± 0.04°C (Figure S4). Overall, the average depth of the temperature minimum defined here is prone to underestimation due to the entrainment of oceanic heat stored below the winter mixed layer. Input of freshwater can also lower the salinity below that of the actual temperature minimum, although entrainment of more saline water from below is more likely. This would also explain part of the difference in freezing point temperatures. How these uncertainties reflect on the assumed remnant winter nutrient concentrations at these depths is difficult to assess since there are very few recently measured winter concentrations available for comparison (Table S3).

#### 5.3.4. Biological Oxygen Supersaturation

In the calculations of $NCP_{O2/Ar}$, Ar is assumed to be at saturation. Under open ocean conditions, Ar can deviate from saturation by a few percent [*Shadwick et al*., 2014; *Eveleth et al*., 2014], introducing an error of this magnitude in the NCP estimates [*Cassar et al*., 2011]. Under sea ice, deviation from saturation has been found to be more significant (up to 7% undersaturation during ARK-XXVI/3 reported by *Eveleth et al.* [2014]). Although this error can be accounted for by concurrent optode measurements, this is a small error compared to the other sources of uncertainty described below.

One intrinsic assumption associated with the conventional application of the $\Delta(O_2/Ar)$ approach for estimating NCP is that the biological $O_2$ efflux to the atmosphere balances NCP. In other words, the change in the biological oxygen inventory in the surface is assumed to be small relative to the flux to the atmosphere. This assumption is sometimes violated [e.g., *Hamme et al*., 2012; *Martin et al*., 2013] and likely violated within the ice-covered central Arctic Ocean. Under such conditions, NCP is best approximated by

$$\mathrm{NCP}_{\mathrm{O_2/Ar}}\left(\mathrm{mmol\ C\ m^{-2}\ d^{-1}}\right) = \frac{1}{\mathrm{O_2:C}}\left[k_{\mathrm{O_2}}\cdot[\mathrm{O_2}]_{\mathrm{sat}}\cdot\Delta(\mathrm{O_2/Ar}) + \mathrm{MLD}\frac{\mathrm{d}\left([\mathrm{O_2}]_{\mathrm{sat}}\cdot\Delta(\mathrm{O_2/Ar})\right)}{\mathrm{d}t}\right] \quad (11)$$

where the last term on the right-hand side accounts for the time rate of change in the biological oxygen inventory within the mixed layer. Because we have no time series information, we cannot account for this term which could be substantial under sea ice. Another source of error is the vertical mixing of oxygen-depleted waters, which is poorly constrained in the region, but vertical mixing is mostly strongly limited due to strong stratification. However, not accounting for both of these processes can lead to biases when computing NCP.

An additional significant and poorly constrained source of uncertainty is associated with gas transfer reconstructions. Some of the spatial variability observed during our cruise can potentially be attributed to

differences in gas exchange. The influence of wind speed history on piston velocity has recently been explored by *Bender et al*. [2011]. Errors associated with the gas transfer velocity parameterization based on wind speed [e.g., *Sweeney et al*., 2007; *Wanninkhof and McGillis*, 1999] are likely of minor importance compared to the influence of ice cover on gas exchange in the region of our study.

#### 5.3.5. Sea Ice

Local sea ice features such as leads of open water and melt ponds can enhance productivity [*Gosselin et al*., 1997; *Sakshaug*, 2004] and $CO_2$ gas exchange [*Else et al*., 2013]. Small-scale features are not taken into account in the satellite-derived sea ice concentration along the transects and in the applied sea ice correction of the gas transfer velocity. In the sea ice-covered deep basins, no clear correlations were found between NCP or $\Delta(O_2/Ar)$ with respect to sea ice concentration, sea ice type, surface solar irradiance, or heat input through sea ice and ocean, with the exception of the peak over the Mendeleev Ridge which corresponds to the region of highest light transmittance through thin first-year ice. The physical properties were acquired for the transects through interpolation of Arctic-wide maps (upscaled, 10 km grid) as given by *Nicolaus et al*. [2012] for August 2011. The lack of correlation might be due to differences in spatial and temporal resolution between the methods and data sets or the fact that sea ice is dynamic (e.g., drifting, sea ice melt, and melt ponds) throughout the productive season. Another alternative is that the signature of NCP in the water column is integrated over a time period when the water has transited an area of diverse sea ice coverage.

## 6. Summary and Conclusions

Large-scale patterns of NCP were derived using four approaches for the deep basins of the Arctic Ocean during late summer. Even if large uncertainties are associated with the approaches, it is obvious that there is a large variability in NCP over the studied area: the spatial distribution revealed by the different approaches is quite similar. Much of the spatial variability and magnitude can be ascribed to the complex and heterogeneous hydrographic and biogeochemical structure of the upper layers of the Arctic Ocean, both leading to different biological regimes. This variability is likely a function of sea ice concentration, vertical mixing, and water mass circulation, all of which are predicted to change in the future. The sea ice concentration impact NCP by attenuating light conditions in the underlying waters, while vertical mixing and water mass circulation contribute to the nutrient supply.

High rates of late summer NCP (up to 6 mol C $m^{-2}$) were observed at the ice edge and shelf break north of Franz Josef Land and Severnaya Zemlya. Low values ($<$1 mol C $m^{-2}$) were found in the sea ice-covered deep basins, with a strong spatial variability. Lowest values were found in the Amundsen Basin. Moderate NCP were observed in the Nansen and Makarov Basins, with slightly higher estimates over the Mendeleev Ridge. The ice-edge regime is a special feature where several conditions may promote NCP. First, a wind parallel to the ice edge promotes upwelling, supplying new nutrients. Second, the withdrawal of the ice during the productive season exposes surface water of higher nutrient concentrations. Both the nutrients and light availability may lead to the higher NCP observed at the marginal ice zone.

Nutrient concentrations were close to depletion in the shallow surface layer. Surface $pCO_2$ was consistently undersaturated with respect to the atmosphere (but highly variable) and mirrored the $\Delta(O_2/Ar)$ with a high negative correlation, consistent with the notion that biology is the main driver of $pCO_2$ variations. It should be noted that the signature of the waters in the central Arctic Ocean is slightly modified during its route to the region. It is not possible to pinpoint the location of all the processes causing this signature. Surface waters along most transects were net autotrophic on a time scale of the residence time of oxygen under the ice. An apparent peak in $\Delta(O_2/Ar)$ was observed just south of the Gakkel Ridge in the Nansen Basin and may result from an eddy-like feature that weakens the halocline, allowing nutrients to be transported into the surface layer. An alternative explanation is topographically induced mixing connected to the crossing of a shallow seamount at the Gakkel Ridge.

Our study presents high-resolution and large-scale interbasin NCP variability within the central Arctic Ocean. Our observations thereby provide further constraints on biological activity in the understudied sea ice-covered region and may help with the increasing effort to model the central Arctic Ocean biogeochemistry.

Our findings support a coupling of NCP to sea ice coverage and nutrient supply and thus stress a potential change in spatial and temporal distribution of NCP in a future Arctic Ocean. In a situation with substantial

decrease in summer sea ice coverage, it is highly likely that the NCP will change both in magnitude and in the spatial distribution. To follow the evolution of NCP in space and time, it is suggested to apply one or several of these approaches in shipboard investigations with a time interval of 3 to 5 years. In the future these studies may be achievable by employing autonomous platforms, but at present all the sensors needed do not have the quality necessary for these investigations in the ice-covered Arctic Ocean.

**Acknowledgments**

The data for this paper are available according to: physical oceanography data [*Schauer et al*., 2011]; carbonate system data [*Anderson et al*., 2011]; nutrient data, to be submitted to PANGAEA (http://www.pangaea.de/); underway $pCO_2$ data, submitted to SOCAT version 3 (release in 2015); underway $O_2$/Ar data [*Eveleth et al*., 2014]. NCP results in Figure 5 are made available in the associated supporting information. Ancillary data used in this paper are referred to by their source in the text. We thank the supporting crew and Master of R/V *Polarstern*, chief scientist Ursula Schauer, and the AWI Sea Ice Physics group. We are grateful to Kai-Uwe Ludwichowski and Claudia Burau for nutrient measurements and Anders Karlsson for valuable data analysis. This research was supported by grants from the Swedish Research Council Formas (project reference 214-2008-1383), the Swedish Research Council (contract 621-2010-4084), the European Union projects CarboChange (project reference 264879) and EPOCA (project reference 211384), the Royal Swedish Academy of Sciences, and the YMER-80 Foundation. N.C. was partly supported by an Alfred P. Sloan fellowship. M.K. received financial support from the Väisälä Foundation and the European Union Seventh Framework Program NACLIM (grant agreement 308299). We would like to thank two anonymous reviewers for their comments that helped improve the manuscript.

## References

Amante, C., and B. W. Eakins (2009), ETOPO1 1 arc-minute global relief model: Procedures, data sources and analysis, *NOAA Tech. Memo., NESDIS NGDC-24*, 19.

Anderson, L. A., and J. L. Sarmiento (1994), Redfield ratios of remineralization determined by nutrient data analysis, *Global Biogeochem. Cycles*, *8*(1), 65–80, doi:10.1029/93GB03318.

Anderson, L. G., E. P. Jones, and J. H. Swift (2003), Export production in the central Arctic Ocean evaluated from phosphate deficits, *J. Geophys. Res.*, *108*(C6), 3199, doi:10.1029/2001JC001057.

Anderson, L. G., E. Falck, E. P. Jones, S. Jutterström, and J. H. Swift (2004a), Enhanced uptake of atmospheric $CO_2$ during freezing of seawater: A field study in Storfjorden, Svalbard, *J. Geophys. Res.*, *109*, C06004, doi:10.1029/2003JC002120.

Anderson, L. G., S. Jutterström, S. Kaltin, E. P. Jones, and G. Björk (2004b), Variability in river runoff distribution in the Eurasian Basin of the Arctic Ocean, *J. Geophys. Res.*, *109*, C01016, doi:10.1029/2003JC001773.

Anderson, L. G., T. Tanhua, G. Björk, S. Hjalmarsson, E. P. Jones, S. Jutterström, B. Rudels, J. H. Swift, and I. Wåhlström (2010), Arctic ocean shelf–basin interaction: An active continental shelf $CO_2$ pump and its impact on the degree of calcium carbonate solubility, *Deep Sea Res., Part I*, *57*(7), 869–879, doi:10.1016/j.dsr.2010.03.012.

Anderson, L. G., A. Ulfsbo, and Y. Ericson (2011), Seawater carbonate chemistry in the Arctic Ocean during the F/S Polarstern cruise ARK-XXVI/3, in August-October, 2011. [Available at http://doi.pangaea.de/10.1594/PANGAEA.775817.]

Arrigo, K. R., and G. L. van Dijken (2011), Secular trends in Arctic Ocean net primary production, *J. Geophys. Res.*, *116*, C09011, doi:10.1029/2011JC007151.

Arrigo, K. R., G. van Dijken, and S. Pabi (2008), Impact of a shrinking Arctic ice cover on marine primary production, *Geophys. Res. Lett.*, *35*, L19603, doi:10.1029/2008GL035028.

Arrigo, K. R., et al. (2012), Massive phytoplankton blooms under Arctic sea ice, *Science*, *336*(6087), 1408–1408, doi:10.1126/science.1215065.

Bates, N. R. (2006), Air-sea $CO_2$ fluxes and the continental shelf pump of carbon in the Chukchi Sea adjacent to the Arctic Ocean, *J. Geophys. Res.*, *111*, C10013, doi:10.1029/2005JC003083.

Bates, N. R., and J. T. Mathis (2009), The Arctic Ocean marine carbon cycle: Evaluation of air-sea $CO_2$ exchanges, ocean acidification impacts and potential feedbacks, *Biogeosciences*, *6*(11), 2433–2459, doi:10.5194/bg-6-2433-2009.

Bender, M. L., S. Kinter, N. Cassar, and R. Wanninkhof (2011), Evaluating gas transfer velocity parameterizations using upper ocean radon distributions, *J. Geophys. Res.*, *116*, C02010, doi:10.1029/2009JC005805.

Boetius, A., et al. (2013), Export of algal biomass from the melting Arctic sea ice, *Science*, *339*(6126), 1430–1432, doi:10.1126/science.1231346.

Bourgain, P., J. C. Gascard, J. Shi, and J. Zhao (2013), Large-scale temperature and salinity changes in the upper Canadian Basin of the Arctic Ocean at a time of a drastic Arctic Oscillation inversion, *Ocean Sci.*, *9*(2), 447–460, doi:10.5194/os-9-447-2013.

Cai, W. J., et al. (2010), Decrease in the $CO_2$ uptake capacity in an ice-free Arctic Ocean basin, *Science*, *329*(5991), 556–559, doi:10.1126/science.1189338.

Carmack, E., and D. C. Chapman (2003), Wind-driven shelf/basin exchange on an Arctic shelf: The joint roles of ice cover extent and shelf-break bathymetry, *Geophys. Res. Lett.*, *30*(14), 1778, doi:10.1029/2003GL017526.

Carmack, E., D. Barber, J. Christensen, R. Macdonald, B. Rudels, and E. Sakshaug (2006), Climate variability and physical forcing of the food webs and the carbon budget on panarctic shelves, *Prog. Oceanogr.*, *71*(2–4), 145–181, doi:10.1016/j.pocean.2006.10.005.

Cassar, N., B. A. Barnett, M. L. Bender, J. Kaiser, R. C. Hamme, and B. Tilbrook (2009), Continuous high-frequency dissolved $O_2$/Ar measurements by equilibrator inlet mass spectrometry, *Anal. Chem.*, *81*(5), 1855–1864, doi:10.1021/ac802300u.

Cassar, N., P. J. DiFiore, B. A. Barnett, M. L. Bender, A. R. Bowie, B. Tilbrook, K. Petrou, K. J. Westwood, S. W. Wright, and D. Lefevre (2011), The influence of iron and light on net community production in the Subantarctic and Polar Frontal Zones, *Biogeosciences*, *8*(2), 227–237, doi:10.5194/bg-8-227-2011.

Chierici, M., A. Fransson, and L. G. Anderson (1999), Influence of m-cresol purple indicator additions on the pH of seawater samples: Correction factors evaluated from a chemical speciation model, *Mar. Chem.*, *65*(3–4), 281–290, doi:10.1016/S0304-4203(99)00020-1.

Clayton, T. D., and R. H. Byrne (1993), Spectrophotometric seawater pH measurements: Total hydrogen ion concentration scale calibration of m-cresol purple and at-sea results, *Deep Sea Res., Part I*, *40*(10), 2115–2129, doi:10.1016/0967-0637(93)90048-8.

Codispoti, L. A., V. Kelly, A. Thessen, P. Matrai, S. Suttles, V. Hill, M. Steele, and B. Light (2013), Synthesis of primary production in the Arctic Ocean: III. Nitrate and phosphate based estimates of net community production, *Prog. Oceanogr.*, *110*, 126–150, doi:10.1016/j.pocean.2012.11.006.

Cooper, L. W., J. W. McClelland, R. M. Holmes, P. A. Raymond, J. J. Gibson, C. K. Guay, and B. J. Peterson (2008), Flow-weighted values of runoff tracers ($\delta^{18}O$, DOC, Ba, alkalinity) from the six largest Arctic rivers, *Geophys. Res. Lett.*, *35*, L18606, doi:10.1029/2008GL035007.

Craig, H., and T. Hayward (1987), Oxygen supersaturation in the ocean: Biological versus physical contributions, *Science*, *235*(4785), 199–202, doi:10.1126/science.235.4785.199.

Cross, J. N., J. T. Mathis, and N. R. Bates (2012), Hydrographic controls on net community production and total organic carbon distributions in the eastern Bering Sea, *Deep Sea Res., Part II*, *65–70*, 98–109, doi:10.1016/j.dsr2.2012.02.003.

Cross, J. N., J. T. Mathis, N. R. Bates, and R. H. Byrne (2013), Conservative and non-conservative variations of total alkalinity on the southeastern Bering Sea shelf, *Mar. Chem.*, *154*, 100–112, doi:10.1016/j.marchem.2013.05.012.

Dickson, A. G. (1990), Standard potential of the reaction: $AgCl(s) + 1/2H_2(g) = Ag(s) + HCl(aq)$, and the standard acidity constant of the ion $HSO_4^-$ in synthetic sea water from 273.15 to 318.15 K, *J. Chem. Thermodyn.*, *22*(2), 113–127, doi:10.1016/0021-9614(90)90074-Z.

Dickson, A. G. (1993), The measurement of sea water pH, *Mar. Chem.*, *44*(2–4), 131–142, doi:10.1016/0304-4203(93)90198-W.

Dickson, A. G., C. L. Sabine, and J. R. Christian (2007), *Guide to Best Practices for Ocean $CO_2$ Measurements*, edited, p. 173, North Pacific Marine Science Organization (PICES), Sidney, British Columbia, Canada.

Ekwurzel, B., P. Schlosser, R. A. Mortlock, R. G. Fairbanks, and J. H. Swift (2001), River runoff, sea ice meltwater, and Pacific water distribution and mean residence times in the Arctic Ocean, *J. Geophys. Res.*, *106*(C5), 9075–9092, doi:10.1029/1999JC000024.

Else, B. G. T., T. N. Papakyriakou, R. J. Galley, W. M. Drennan, L. A. Miller, and H. Thomas (2011), Wintertime $CO_2$ fluxes in an Arctic polynya using eddy covariance: Evidence for enhanced air-sea gas transfer during ice formation, *J. Geophys. Res.*, *116*, C00G03, doi:10.1029/2010JC006760.

Else, B. G. T., T. N. Papakyriakou, M. G. Asplin, D. G. Barber, R. J. Galley, L. A. Miller, and A. Mucci (2013), Annual cycle of air-sea $CO_2$ exchange in an Arctic polynya region, *Global Biogeochem. Cycles*, *27*, 388–398, doi:10.1002/gbc.20016.

Emerson, S., P. Quay, C. Stump, D. Wilbur, and M. Knox (1991), $O_2$, Ar, $N_2$, and $^{222}Rn$ in surface waters of the subarctic Ocean: Net biological $O_2$ production, *Global Biogeochem. Cycles*, *5*(1), 49–69, doi:10.1029/90GB02656.

Ericson, Y., A. Ulfsbo, S. van Heuven, G. Kattner, and L. G. Anderson (2014), Increasing carbon inventory of the intermediate layers of the Arctic Ocean, *J. Geophys. Res. Oceans*, *119*, 2312–2326, doi:10.1002/2013JC009514.

Eveleth, R., M.-L. Timmermans, and N. Cassar (2014), Physical and biological controls on oxygen saturation variability in the upper Arctic Ocean, *J. Geophys. Res. Oceans*, doi:10.1002/2014JC009816.

Falkowski, P., E. Laws, R. Barber, and J. Murray (2003), Phytoplankton and their role in primary, new, and export production, in *Ocean Biogeochemistry*, edited by M. R. Fasham, pp. 99–121, Springer, Berlin Heidelberg, 978-3-642-62691-3.

Fransson, A., M. Chierici, L. G. Anderson, I. Bussmann, G. Kattner, E. Peter Jones, and J. H. Swift (2001), The importance of shelf processes for the modification of chemical constituents in the waters of the Eurasian Arctic Ocean: Implication for carbon fluxes, *Cont. Shelf Res.*, *21*(3), 225–242, doi:10.1016/S0278-4343(00)00088-1.

Fransson, A., M. Chierici, and Y. Nojiri (2009), New insights into the spatial variability of the surface water carbon dioxide in varying sea ice conditions in the Arctic Ocean, *Cont. Shelf Res.*, *29*(10), 1317–1328, doi:10.1016/j.csr.2009.03.008.

Fransson, A., M. Chierici, L. A. Miller, G. Carnat, E. Shadwick, H. Thomas, S. Pineault, and T. N. Papakyriakou (2013), Impact of sea-ice processes on the carbonate system and ocean acidification at the ice-water interface of the Amundsen Gulf, Arctic Ocean, *J. Geophys. Res. Oceans*, *118*, 7001–7023, doi:10.1002/2013JC009164.

Frigstad, H., T. Andersen, R. G. J. Bellerby, A. Silyakova, and D. O. Hessen (2014), Variation in the seston C:N ratio of the Arctic Ocean and pan-Arctic shelves, *J. Mar. Syst.*, *129*, 214–223, doi:10.1016/j.jmarsys.2013.06.004.

Friis, K., A. Körtzinger, and D. W. R. Wallace (2003), The salinity normalization of marine inorganic carbon chemistry data, *Geophys. Res. Lett.*, *30*(2), 1085, doi:10.1029/2002GL015898.

Garcia, H. E., and L. I. Gordon (1992), Oxygen solubility in seawater: Better fitting options, *Limnol. Oceanogr.*, *37*(6), 1307–1312.

Gosselin, M., M. Levasseur, P. A. Wheeler, R. A. Horner, and B. C. Booth (1997), New measurements of phytoplankton and ice algal production in the Arctic Ocean, *Deep Sea Res., Part II*, *44*(8), 1623–1644, doi:10.1016/S0967-0645(97)00054-4.

Hamme, R. C., et al. (2012), Dissolved $O_2$/Ar and other methods reveal rapid changes in productivity during a Lagrangian experiment in the Southern Ocean, *J. Geophys. Res.*, *117*, C00F12, doi:10.1029/2011JC007046.

Haraldsson, C., L. G. Anderson, M. Hassellöv, S. Hulth, and K. Olsson (1997), Rapid, high-precision potentiometric titration of alkalinity in ocean and sediment pore waters, *Deep Sea Res., Part I*, *44*(12), 2031–2044, doi:10.1016/S0967-0637(97)00088-5.

Holmes, R., et al. (2012), Seasonal and annual fluxes of nutrients and organic matter from large rivers to the Arctic Ocean and surrounding seas, *Estuaries Coasts*, *35*(2), 369–382, doi:10.1007/s12237-011-9386-6.

Hoppema, M., and L. Goeyens (1999), Redfield behavior of carbon, nitrogen, and phosphorus depletions in Antarctic surface water, *Limnol. Oceanogr.*, *44*(1), 220–224, doi:10.4319/lo.1999.44.1.0220.

Hoppema, M., L. Goeyens, and E. Fahrbach (2000), Intense nutrient removal in the remote area off Larsen Ice Shelf (Weddell Sea), *Polar Biol.*, *23*(2), 85–94, doi:10.1007/s003000050012.

Hoppema, M., R. Middag, H. W. Baar, E. Fahrbach, E. Weerlee, and H. Thomas (2007), Whole season net community production in the Weddell Sea, *Polar Biol.*, *31*(1), 101–111, doi:10.1007/s00300-007-0336-5.

Ishii, M., H. Y. Inoue, and H. Matsueda (2002), Net community production in the marginal ice zone and its importance for the variability of the oceanic $pCO_2$ in the Southern Ocean south of Australia, *Deep Sea Res., Part II*, *49*(9–10), 1691–1706, doi:10.1016/S0967-0645(02)00007-3.

Jennings, J. C., L. I. Gordon, and D. M. Nelson (1984), Nutrient depletion indicates high primary productivity in the Weddell Sea, *Nature*, *309*, 51–54.

Johnson, K. M., J. M. Sieburth, P. J. L. Williams, and L. Brändström (1987), Coulometric total carbon dioxide analysis for marine studies: Automation and calibration, *Mar. Chem.*, *21*(2), 117–133, doi:10.1016/0304-4203(87)90033-8.

Jones, E. P., and L. G. Anderson (1986), On the origin of the chemical properties of the Arctic Ocean halocline, *J. Geophys. Res.*, *91*(C9), 10,759–10,767, doi:10.1029/JC091iC09p10759.

Jones, E. P., L. G. Anderson, and J. H. Swift (1998), Distribution of Atlantic and Pacific waters in the upper Arctic Ocean: Implications for circulation, *Geophys. Res. Lett.*, *25*(6), 765–768, doi:10.1029/98GL00464.

Karcher, M., J. N. Smith, F. Kauker, R. Gerdes, and W. M. Smethie (2012), Recent changes in Arctic Ocean circulation revealed by iodine-129 observations and modeling, *J. Geophys. Res.*, *117*, C08007, doi:10.1029/2011JC007513.

Korhonen, M., B. Rudels, M. Marnela, A. Wisotzki, and J. Zhao (2013), Time and space variability of freshwater content, heat content and seasonal ice melt in the Arctic Ocean from 1991 to 2011, *Ocean Sci.*, *9*(6), 1015–1055, doi:10.5194/os-9-1015-2013.

Krishfield, R., J. Toole, A. Proshutinsky, and M. L. Timmermans (2008), Automated ice-tethered profilers for seawater observations under pack ice in all seasons, *J. Atmos. Oceanic Tech.*, *25*(11), 2091–2105, doi:10.1175/2008JTECHO587.1.

Lansard, B., A. Mucci, L. A. Miller, R. W. Macdonald, and Y. Gratton (2012), Seasonal variability of water mass distribution in the southeastern Beaufort Sea determined by total alkalinity and $\delta^{18}O$, *J. Geophys. Res.*, *117*, C03003, doi:10.1029/2011JC007299.

Laws, E. A. (1991), Photosynthetic quotients, new production and net community production in the open ocean, *Deep Sea Res., Part I*, *38*(1), 143–167, doi:10.1016/0198-0149(91)90059-O.

Laxon, S. W., et al. (2013), CryoSat-2 estimates of Arctic sea ice thickness and volume, *Geophys. Res. Lett.*, *40*, 1–6, doi:10.1002/grl.50193.

Li, W. K. W., F. A. McLaughlin, C. Lovejoy, and E. C. Carmack (2009), Smallest algae thrive as the Arctic Ocean freshens, *Science*, *326*(5952), 539, doi:10.1126/science.1179798.

Long, M. C., R. B. Dunbar, P. D. Tortell, W. O. Smith, D. A. Mucciarone, and G. R. DiTullio (2011), Vertical structure, seasonal drawdown, and net community production in the Ross Sea, Antarctica, *J. Geophys. Res.*, *116*, C10029, doi:10.1029/2009JC005954.

Loose, B., W. R. McGillis, P. Schlosser, D. Perovich, and T. Takahashi (2009), Effects of freezing, growth, and ice cover on gas transport processes in laboratory seawater experiments, *Geophys. Res. Lett.*, *36*, L05603, doi:10.1029/2008GL036318.

Lueck, R. G., and T. D. Mudge (1997), Topographically induced mixing around a shallow seamount, *Science*, *276*(5320), 1831–1833, doi:10.1126/science.276.5320.1831.

Macdonald, R. W., L. G. Anderson, J. P. Christensen, L. A. Miller, I. P. Semiletov, and R. Stein (2009), The Arctic Ocean: Budgets and fluxes, in *Carbon and Nutrient Fluxes in Continental Margins: A Global Synthesis*, edited by K.-K. Liu et al., pp. 291–303, IGBP Book Series, Springer, Berlin.

Martin, P., et al. (2013), Iron fertilization enhanced net community production but not downward particle flux during the Southern Ocean iron fertilization experiment LOHAFEX, *Global Biogeochem. Cycles*, *27*, 871–881, doi:10.1002/gbc.20077.

Mathis, J. T., J. N. Cross, N. R. Bates, S. Bradley Moran, M. W. Lomas, C. W. Mordy, and P. J. Stabeno (2010), Seasonal distribution of dissolved inorganic carbon and net community production on the Bering Sea shelf, *Biogeosciences*, *7*(5), 1769–1787, doi:10.5194/bg-7-1769-2010.

Mauritzen, C. (1996), Production of dense overflow waters feeding the North Atlantic across the Greenland-Scotland Ridge. Part 1: Evidence for a revised circulation scheme, *Deep Sea Res., Part I*, *43*(6), 769–806, doi:10.1016/0967-0637(96)00037-4.

McGuire, A. D., F. S. Chapin, J. E. Walsh, and C. Wirth (2006), Integrated regional changes in Arctic climate feedbacks: Implications for the global climate system*, *Annu. Rev. Env. Res.*, *31*(1), 61–91, doi:10.1146/annurev.energy.31.020105.100253.

Morison, J., R. Kwok, C. Peralta-Ferriz, M. Alkire, I. Rigor, R. Andersen, and M. Steele (2012), Changing Arctic Ocean freshwater pathways, *Nature*, *481*(7379), 66–70, doi:10.1038/nature10705.

Muench, R. D., J. H. Morison, L. Padman, D. Martinson, P. Schlosser, B. Huber, and R. Hohmann (2001), Maud Rise revisited, *J. Geophys. Res.*, *106*, 2423–2440, doi:10.1029/2000JC000531.

Mundy, C. J., et al. (2009), Contribution of under-ice primary production to an ice-edge upwelling phytoplankton bloom in the Canadian Beaufort Sea, *Geophys. Res. Lett.*, *36*, L17601, doi:10.1029/2009GL038837.

Nicolaus, M., C. Katlein, J. Maslanik, and S. Hendricks (2012), Changes in Arctic sea ice result in increasing light transmittance and absorption, *Geophys. Res. Lett.*, *39*, L24501, doi:10.1029/2012GL053738.

Pabi, S., G. L. van Dijken, and K. R. Arrigo (2008), Primary production in the Arctic Ocean, 1998–2006, *J. Geophys. Res.*, *113*, C08005, doi:10.1029/2007JC004578.

Palevsky, H. I., F. Ribalet, J. E. Swalwell, C. E. Cosca, E. D. Cokelet, R. A. Feely, E. V. Armbrust, and P. D. Quay (2013), The influence of net community production and phytoplankton community structure on $CO_2$ uptake in the Gulf of Alaska, *Global Biogeochem. Cycles*, *27*, 664–676, doi:10.1002/gbc.20058.

Perrette, M., A. Yool, G. D. Quartly, and E. E. Popova (2011), Near-ubiquity of ice-edge blooms in the Arctic, *Biogeosciences*, *8*(2), 515–524, doi:10.5194/bg-8-515-2011.

Pfeil, B., et al. (2013), A uniform, quality controlled Surface Ocean $CO_2$ Atlas (SOCAT), *Earth Syst. Sci. Data*, *5*(1), 125–143, doi:10.5194/essd-5-125-2013.

Pierrot, D., C. Neill, K. Sullivan, R. Castle, R. Wanninkhof, H. Lüger, T. Johannessen, A. Olsen, R. A. Feely, and C. E. Cosca (2009), Recommendations for autonomous underway $pCO_2$ measuring systems and data-reduction routines, *Deep Sea Res., Part II*, *56*(8–10), 512–522, doi:10.1016/j.dsr2.2008.12.005.

Pondaven, P., O. Ragueneau, P. Treguer, A. Hauvespre, L. Dezileau, and J. L. Reyss (2000), Resolving the 'opal paradox' in the Southern Ocean, *Nature*, *405*(6783), 168–172.

Popova, E. E., A. Yool, A. C. Coward, Y. K. Aksenov, S. G. Alderson, B. A. de Cuevas, and T. R. Anderson (2010), Control of primary production in the Arctic by nutrients and light: Insights from a high resolution ocean general circulation model, *Biogeosciences*, *7*(11), 3569–3591, doi:10.5194/bg-7-3569-2010.

Popova, E. E., A. Yool, Y. Aksenov, and A. C. Coward (2013), Role of advection in Arctic Ocean lower trophic dynamics: A modeling perspective, *J. Geophys. Res. Oceans*, *118*, 1571–1586, doi:10.1002/jgrc.20126.

Rainville, L., and P. Winsor (2008), Mixing across the Arctic Ocean: Microstructure observations during the Beringia 2005 Expedition, *Geophys. Res. Lett.*, *35*, L08606, doi:10.1029/2008GL033532.

Redfield, A. C., B. H. Ketchum, and F. A. Richards (1963), The influence of organisms on the composition of sea water, in *The Sea*, vol. 2, edited by M. N. Hill, pp. 26–77, Wiley, New York.

Reuer, M. K., B. A. Barnett, M. L. Bender, P. G. Falkowski, and M. B. Hendricks (2007), New estimates of Southern Ocean biological production rates from $O_2$/Ar ratios and the triple isotope composition of $O_2$, *Deep Sea Res., Part I*, *54*(6), 951–974, doi:10.1016/j.dsr.2007.02.007.

Roy, R. N., L. N. Roy, K. M. Vogel, C. Porter-Moore, T. Pearson, C. E. Good, F. J. Millero, and D. M. Campbell (1993), The dissociation constants of carbonic acid in seawater at salinities 5 to 45 and temperatures 0 to 45°C, *Mar. Chem.*, *44*(2–4), 249–267, doi:10.1016/0304-4203(93)90207-5.

Rubin, S. I., T. Takahashi, D. W. Chipman, and J. G. Goddard (1998), Primary productivity and nutrient utilization ratios in the Pacific sector of the Southern Ocean based on seasonal changes in seawater chemistry, *Deep Sea Res., Part I*, *45*(8), 1211–1234, doi:10.1016/S0967-0637(98)00021-1.

Rudels, B., E. P. Jones, L. G. Anderson, and G. Kattner (1994), On the intermediate depth waters of the Arctic Ocean, in *The Polar Oceans and Their Role in Shaping the Global Environment*, edited by O. M. Johannessen, R. D. Muench, and J. E. Overland, pp. 33–46, AGU, Washington, D. C.

Rudels, B., L. G. Anderson, and E. P. Jones (1996), Formation and evolution of the surface mixed layer and halocline of the Arctic Ocean, *J. Geophys. Res.*, *101*(C4), 8807, doi:10.1029/96JC00143.

Rutgers van der Loeff, M. M., N. Cassar, M. Nicolaus, B. Rabe, and I. Stimac (2014), The influence of sea ice cover on air-sea gas exchange estimated with radon-222 profiles, *J. Geophys. Res. Oceans*, *119*, 2735–2751, doi:10.1002/2013JC009321.

Rysgaard, S., R. N. Glud, M. K. Sejr, J. Bendtsen, and P. B. Christensen (2007), Inorganic carbon transport during sea ice growth and decay: A carbon pump in polar seas, *J. Geophys. Res.*, *112*, C03016, doi:10.1029/2006JC003572.

Rysgaard, S., R. N. Glud, K. Lennert, M. Cooper, N. Halden, R. J. G. Leakey, F. C. Hawthorne, and D. Barber (2012), Ikaite crystals in melting sea ice—Implications for *p*CO2 and pH levels in Arctic surface waters, *The Cryosphere*, *6*(4), 901–908, doi:10.5194/tc-6-901-2012.

Sakshaug, E. (2004), Primary and secondary production in the Arctic Seas, in *The Organic Carbon Cycle in the Arctic Ocean*, edited by R. Stein and R. MacDonald, pp. 57–81, Springer, Berlin Heidelberg.

Schauer, U. (2012), *The Expedition of the Research Vessel "Polarstern" to the Arctic in 2011 (ARK-XXVI/3 - TransArc)*, 205 pp., Alfred Wegener Institute for Polar and Marine Research, Bremerhaven, Germany.

Schauer, U., B. Rabe, and A. Wisotzki (2011), Physical oceanography during POLARSTERN cruise ARK-XXVI/3. [Available at http://doi.pangaea.de/10.1594/PANGAEA.774181.]

Semiletov, I. P., I. I. Pipko, N. E. Shakhova, O. V. Dudarev, S. P. Pugach, A. N. Charkin, C. P. McRoy, D. Kosmach, and Ö. Gustafsson (2011), Carbon transport by the Lena River from its headwaters to the Arctic Ocean, with emphasis on fluvial input of terrestrial particulate organic carbon vs. carbon transport by coastal erosion, *Biogeosciences*, *8*(9), 2407–2426, doi:10.5194/bg-8-2407-2011.

Shadwick, E. H., et al. (2011), Seasonal variability of the inorganic carbon system in the Amundsen Gulf region of the southeastern Beaufort Sea, *Limnol. Oceanogr.*, *56*(1), 303–322, doi:10.4319/lo.2011.56.1.0303.

Shadwick, E. H., B. Tilbrook, N. Cassar, T. W. Trull, and S. R. Rintoul (2014), Summertime physical and biological controls on $O_2$ and $CO_2$ in the Australian Sector of the Southern Ocean, *J. Mar. Syst.*, doi:10.1016/j.jmarsys.2013.12.008.

Shaw, W. J., T. P. Stanton, M. G. McPhee, J. H. Morison, and D. G. Martinson (2009), Role of the upper ocean in the energy budget of Arctic sea ice during SHEBA, *J. Geophys. Res.*, *114*, C06012, doi:10.1029/2008JC004991.

Spreen, G., L. Kaleschke, and G. Heygster (2008), Sea ice remote sensing using AMSR-E 89 GHz channels, *J. Geophys. Res.*, *113*, C02S03, doi:10.1029/2005JC003384.

Steele, M., W. Ermold, and J. Zhang (2008), Arctic Ocean surface warming trends over the past 100 years, *Geophys. Res. Lett.*, *35*, L02614, doi:10.1029/2007GL031651.

Steiner, N. S., W. G. Lee, and J. R. Christian (2013), Enhanced gas fluxes in small sea ice leads and cracks: Effects on $CO_2$ exchange and ocean acidification, *J. Geophys. Res. Oceans*, *118*, 1195–1205, doi:10.1002/jgrc.20100.

Sterner, R. W., T. Andersen, J. J. Elser, D. O. Hessen, J. M. Hood, E. McCauley, and J. Urabe (2008), Scale-dependent carbon:nitrogen:phosphorus seston stoichiometry in marine and freshwaters, *Limnol. Oceanogr.*, *53*(3), 1169–1180, doi:10.4319/lo.2008.53.3.1169.

Sweeney, C., E. Gloor, A. R. Jacobson, R. M. Key, G. McKinley, J. L. Sarmiento, and R. Wanninkhof (2007), Constraining global air-sea gas exchange for $CO_2$ with recent bomb $^{14}C$ measurements, *Global Biogeochem. Cycles*, *21*, GB2015, doi:10.1029/2006GB002784.

Takahashi, T., et al. (2002), Global sea–air $CO_2$ flux based on climatological surface ocean $pCO_2$, and seasonal biological and temperature effects, *Deep Sea Res., Part II*, *49*(9–10), 1601–1622, doi:10.1016/S0967-0645(02)00003-6.

Takahashi, T., et al. (2009), Climatological mean and decadal change in surface ocean $pCO_2$, and net sea–air $CO_2$ flux over the global oceans, *Deep Sea Res., Part II*, *56*(8–10), 554–577, doi:10.1016/j.dsr2.2008.12.009.

Tamelander, T., A. B. Aubert, and C. Wexels Riser (2012), Export stoichiometry and contribution of copepod faecal pellets to vertical flux of particulate organic carbon, nitrogen and phosphorus, *Mar. Ecol. Prog. Ser.*, *459*, 17–28, doi:10.3354/meps09733.

Tanhua, T., E. P. Jones, E. Jeansson, S. Jutterström, W. M. Smethie, D. W. R. Wallace, and L. G. Anderson (2009), Ventilation of the Arctic Ocean: Mean ages and inventories of anthropogenic $CO_2$ and CFC-11, *J. Geophys. Res.*, *114*, C01002, doi:10.1029/2008JC004868.

Timmermans, M. L., J. Toole, A. Proshutinsky, R. Krishfield, and A. Plueddemann (2008), Eddies in the Canada Basin, Arctic Ocean, observed from ice-tethered profilers, *J. Phys. Oceanogr.*, *38*(1), 133–145, doi:10.1175/2007JPO3782.1.

Tremblay, J.-É., and J. Gagnon (2009), The effects of irradiance and nutrient supply on the productivity of Arctic waters: A perspective on climate change, in *Influence of Climate Change on the Changing Arctic and Sub-Arctic Conditions*, edited by J. J. Nihoul and A. Kostianoy, pp. 73–93, Springer, Netherlands.

Tremblay, J.-É., K. Simpson, J. Martin, L. Miller, Y. Gratton, D. Barber, and N. M. Price (2008), Vertical stability and the annual dynamics of nutrients and chlorophyll fluorescence in the coastal, southeast Beaufort Sea, *J. Geophys. Res.*, *113*, C07S90, doi:10.1029/2007JC004547.

Vancoppenolle, M., L. Bopp, G. Madec, J. Dunne, T. Ilyina, P. R. Halloran, and N. Steiner (2013), Future Arctic Ocean primary productivity from CMIP5 simulations: Uncertain outcome, but consistent mechanisms, *Global Biogeochem. Cycles*, *27*, 605–619, doi:10.1002/gbc.20055.

van Heuven, S., D. Pierrot, E. Lewis, and D. W. R. Wallace (2009), MATLAB Program developed for $CO_2$ system calculations, version 1.1 2011, ORNL/CDIAC-105b, Carbon Dioxide Inf. Anal. Cent., Oak Ridge Natl. Lab., U.S. Dep. of Energy, Oak Ridge, Tenn.

VLIZ (2011), Maritime Boundaries Geodatabase, version 6. [Available at http://www.marineregions.org.]

Wanninkhof, R. (1992), Relationship between wind speed and gas exchange over the ocean, *J. Geophys. Res.*, *97*(C5), 7373–7382, doi:10.1029/92JC00188.

Wanninkhof, R., and W. R. McGillis (1999), A cubic relationship between air-sea $CO_2$ exchange and wind speed, *Geophys. Res. Lett.*, *26*(13), 1889–1892, doi:10.1029/1999GL900363.

Wassmann, P., et al. (2006), Food webs and carbon flux in the Barents Sea, *Prog. Oceanogr.*, *71*(2–4), 232–287, doi:10.1016/j.pocean.2006.10.003.

Weingartner, T., K. Aagaard, R. Woodgate, S. Danielson, Y. Sasaki, and D. Cavalieri (2005), Circulation on the north central Chukchi Sea shelf, *Deep Sea Res., Part II*, *52*(24–26), 3150–3174, doi:10.1016/j.dsr2.2005.10.015.

Yamamoto-Kawai, M., N. Tanaka, and S. Pivovarov (2005), Freshwater and brine behaviors in the Arctic Ocean deduced from historical data of $\delta^{18}O$ and alkalinity (1929–2002 A.D.), *J. Geophys. Res.*, *110*, C10003, doi:10.1029/2004JC002793.